

Bounds on R-parity Violating Couplings at the Grand Unification Scale from Neutrino Masses

H. K. Dreiner*

*Bethe Center for Theoretical Physics and Physikalisches Institut, Universität Bonn, Bonn, Germany and
SCIPP, University of California Santa Cruz, Santa Cruz, CA 95064, USA*

M. Hanussek†

Bethe Center for Theoretical Physics and Physikalisches Institut, Universität Bonn, Bonn, Germany

S. Grab‡

SCIPP, University of California Santa Cruz, Santa Cruz, CA 95064, USA

We consider the embedding of the supersymmetric Standard Model with broken R-parity in the minimal supergravity (mSUGRA) model. We restrict ourselves to the case of broken lepton number, the B_3 mSUGRA model. We first study in detail how the tree-level neutrino mass depends on the mSUGRA parameters. We find in particular a strong dependence on the trilinear supersymmetry breaking A -parameter, even in the vicinity of the mSUGRA SPS1a point. We then reinvestigate the bounds on the trilinear R-parity violating couplings at the unification scale from the low-energy neutrino masses including dominant one-loop contributions. These bounds were previously shown to be very strict, as low as $\mathcal{O}(10^{-6})$ for SPS1a. We show that these bounds are significantly weakened when considering the full mSUGRA parameter space. In particular the ratio between the tree-level and 1-loop neutrino masses is reduced such that it may agree with the observed neutrino mass hierarchy. We discuss in detail how and in which parameter regions this effect arises.

I. INTRODUCTION

The experimental observation of neutrino oscillations, and thus of neutrino masses, is an experimental indication that the Standard Model of particle physics (SM) is incomplete [1–7].

Experimentally, neutrinos must be relatively light. Direct laboratory measurements restrict their masses to be below $\mathcal{O}(10 \text{ MeV} - 1 \text{ eV})$ [7–12], depending on the flavor. Cosmological observations even give upper bounds of $\mathcal{O}(0.1 \text{ eV})$ on the sum of the neutrino masses [7, 12–14]. Furthermore, the atmospheric and solar neutrino oscillation data are best fit if the squared neutrino mass differences are $\mathcal{O}(10^{-3} \text{ eV}^2)$ and $\mathcal{O}(10^{-5} \text{ eV}^2)$, respectively [7, 15]. This allows for one massless neutrino.

In principle, it is easy to extend the SM Lagrangian by a Dirac neutrino mass term [7]. However, right-handed neutrinos and new Yukawa couplings of $\mathcal{O}(\lesssim 10^{-12})$ are in this case needed. Such tiny couplings seem to be very unnatural and might point towards a dynamical mechanism, that explains the small neutrino masses. Furthermore, the right-handed neutrinos can have an unspecified Majorana neutrino mass.

Most prominently discussed are extensions of the SM involving the see-saw mechanism, by introducing right-handed neutrinos and fixing the new Majorana neutrino mass scale to be large, *cf.* Refs. [7, 16–21].

The see-saw mechanism is also naturally incorporated into supersymmetry (SUSY) [22, 23].

Supersymmetry is one of the most promising extensions of the SM. It is the unique extension of the Lorentz spacetime symmetry, when allowing for graded Lie algebras [24, 25]. Furthermore, it provides a solution to the hierarchy problem of the SM [26–30]. More importantly here: neutrino masses can be generated without introducing right-handed neutrinos if lepton number is violated, *cf.* for example Refs. [31–41].

The most general gauge invariant and renormalizable superpotential of the supersymmetric extension of the SM with minimal particle content (SSM) possesses lepton number conserving (LNC) terms [42, 43]

$$W_{\text{LNC}} = \epsilon_{ab} [(\mathbf{Y}_E)_{ij} L_i^a H_d^b \bar{E}_j + (\mathbf{Y}_D)_{ij} Q_i^{ax} H_d^b \bar{D}_{jx} + (\mathbf{Y}_U)_{ij} Q_i^{ax} H_u^b \bar{U}_{jx} - \mu H_d^a H_u^b] \quad (1)$$

and also lepton number violating (LNV) terms

$$W_{\text{LNV}} = \epsilon_{ab} \left[\frac{1}{2} \lambda_{ijk} L_i^a L_j^b \bar{E}_k + \lambda'_{ijk} L_i^a Q_j^{xb} \bar{D}_{kx} \right] - \epsilon_{ab} \kappa_i L_i^a H_u^b, \quad (2)$$

where $i, j, k = 1, 2, 3$ are generation indices. We have employed the standard notation of Ref. [44].

The LNV interactions violate the discrete symmetries R-parity and proton-hexality (P_6), however, they conserve baryon triality (B_3) [45–48]. Note that B_3 stabilizes the proton because it suppresses the baryon number violating interactions. R-parity, P_6 and B_3 are the only discrete symmetries, which can be written as a remnant of a broken anomaly free gauge symmetry [45–48]. In the following, we assume that

*dreiner@th.physik.uni-bonn.de

†hanussek@th.physik.uni-bonn.de

‡sgrab@scipp.ucsc.edu

B_3 is conserved and thus R-parity and P_6 are violated. Eq. (1) and Eq. (2) constitute the full renormalizable superpotential allowed by this symmetry. For reviews of such theories see for example Refs. [49–51].

Beside the superpotential, also the soft-breaking Lagrangian of the B_3 conserving SSM exhibits lepton number violating operators [52]

$$\begin{aligned}
 -\mathcal{L}_{\text{soft}}^{\text{LNV}} = & \epsilon_{ab} \left[\frac{1}{2} h_{ijk} \tilde{L}_i^a \tilde{L}_j^b \tilde{E}_k + h'_{ijk} \tilde{L}_i^a \tilde{Q}_j^b \tilde{D}_k + \text{h.c.} \right] \\
 & - \epsilon_{ab} \tilde{D}_i \tilde{L}_i^a h_u^b + \text{h.c.} + (h_d^*)^a \mathbf{m}_{h_d \tilde{L}_i}^2 \tilde{L}_i^a,
 \end{aligned} \tag{3}$$

where again $i, j, k = 1, 2, 3$ are generation indices. \tilde{L} , \tilde{E} , \tilde{Q} and \tilde{D} are the scalar components of the lepton doublet, lepton singlet, quark doublet and down quark singlet superfield, respectively. Furthermore, h_u (h_d) denotes the up-type (down-type) scalar Higgs field. Beside the term proportional to $\mathbf{m}_{h_d \tilde{L}_i}^2$, the operators in Eq. (3) are the soft-breaking analog of the terms in Eq. (2).

The LNV terms in Eq. (2) and Eq. (3) lead to the dynamical generation of neutrino masses. For example, the bilinear terms in Eq. (2) mix the Higgsinos, the supersymmetric partners of the Higgs bosons, with the neutrino fields and thus generate one non-vanishing neutrino mass at tree-level [31–33, 37–40].

In this paper, we derive bounds on the trilinear LNV couplings of the superpotential, Eq. (2), from the upper cosmological bound on the sum of neutrino masses [13, 14], *i.e.*

$$\sum m_{\nu_i} < 0.40 \text{ eV}, \tag{4}$$

at 99.9% confidence level. The bound was determined by a combination of the Wilkinson Microwave Anisotropy Probe (WMAP) and Large Scale Structure (LSS) data.

In order to perform a systematic study, we restrict ourselves to the well motivated framework of the B_3 minimal supergravity model (mSUGRA) [52], which provides simple boundary conditions for the SSM parameters at the grand unification scale (M_{GUT}). We describe the model in the next section in detail. We employ the full set of renormalization group equations (RGEs) at one loop [52–55] in order to obtain the B_3 SSM spectrum and the neutrino masses at the electroweak scale (M_{EW}). We then derive bounds on the LNV trilinear couplings at M_{GUT} .

Bounds on trilinear LNV couplings within this model were also derived in Ref. [52] from the generation of neutrino masses at tree-level. It was claimed that neutrino masses put an upper bound of $\mathcal{O}(10^{-3} - 10^{-6})$ on most of the trilinear couplings in Eq. (2). However, it was shown in Ref. [54] that the tree-level neutrino mass can vanish in certain regions of the B_3 mSUGRA parameter space. In our analysis, we especially focus on these regions of parameter space. We

show that the bounds on the trilinear couplings can be weakened up to $\mathcal{O}(10^{-1})$, depending on the boundary conditions.

We go beyond the former work in several aspects. Beside the tree-level neutrino mass, we also include the dominant contributions to the neutrino mass matrix at one-loop. These contributions were neither included in the calculation of the bounds in Ref. [52] nor in Ref. [54]. However, as we show in Sec. IV, the loops dominate in the regions of parameter space where the tree-level mass vanishes. They must thus be included when determining the bounds.

In Ref. [54] there is only a brief explanation of the dominant effect that leads to a vanishing tree-level mass in B_3 mSUGRA. We give for the first time a detailed and complete explanation of how different configurations of the B_3 mSUGRA parameters at M_{GUT} can affect the tree-level *and* loop contributions to the neutrino masses at M_{EW} . Although we restrict ourself to the framework of B_3 mSUGRA, the mechanisms described in this publication also work in more general models. Furthermore, we calculate bounds for *all* trilinear LNV couplings, whereas Ref. [54] focused only on the couplings λ_{i33} and λ'_{i33} . We also update the bounds given in Ref. [52] according to the more recent and stronger bound on the sum of neutrino masses, *cf.* Eq. (4).

Going beyond the work presented here, we believe our results can help find LNV SUSY scenarios that explain the observed neutrino masses and mixing angles. Within the framework of B_3 mSUGRA, Ref. [41] searched for a minimal set of LNV parameters which can explain the measured neutrino parameters. They found sets of five parameters [two trilinear LNV couplings together with the three mixing angles that describe the lepton Yukawa matrix, *cf.* Eq. (1)] that give the right masses and mixing angles. Ref. [41] claimed that the tree-level mass is always much larger than the loop induced masses. But we show in the following, that the loops can exceed the tree-level masses in B_3 mSUGRA. Therefore, it should be possible to find a smaller set of LNV parameters that lies in this region of parameter space and thus posses much larger LNV couplings than those found in Ref. [41]. However, an investigation of the complete neutrino sector is beyond the scope of this paper and will be postponed to a future publication.

We finally note that (large) trilinear LNV couplings can lead to distinct collider signatures at the Large Hadron Collider (LHC), *e.g.*

- Supersymmetric particles (sparticles) can be produced singly at a collider, possibly on resonance [51, 56–63]. For example, single resonant slepton production at the LHC via λ'_{ijk} , Eq. (2) [56–58, 60, 63]. An excess over the SM backgrounds is visible if $\lambda'_{ijk} \gtrsim \mathcal{O}(10^{-3})$, depending also on the sparticle masses [57, 58, 63, 64].
- A LNV coupling λ_{ijk} (λ'_{ijk}) of $\gtrsim \mathcal{O}(10^{-2})$ at

M_{GUT} can significantly change the running of the sparticle masses, such that the scalar electron or muon (sneutrino) is the LSP [52, 65–68]. This can dramatically change the SUSY collider signatures, because (heavy) sparticles normally cascade decay down to the LSP [66, 69].

Note that the generation of neutrino masses via the bilinear terms in Eq. (2) and the corresponding collider signatures have also been investigated; see for example Refs. [70–81] and references therein.

This paper is organized as follows. In Sec. II, we review the parts of the B_3 mSUGRA model that are relevant for this work. Sec. III then shows the different contributions to the neutrino mass matrix that we employ to derive the bounds. We explain the main mechanism leading to a vanishing tree-level neutrino mass in B_3 mSUGRA in Sec. IV and derive the bounds on the LNV trilinear couplings in Sec. V. These sections are the central part of our paper. We conclude in Sec. VI.

App. A explains the additional subleading dependence of the neutrino masses on the B_3 mSUGRA parameter not described in Sec. IV.

II. THE B_3 MSUGRA MODEL

The general B_3 SSM has more than 200 free parameters [82]. This large number is intractable for detailed phenomenological studies. For that purpose the simplifying B_3 mSUGRA model was proposed in Ref. [52], which we now discuss.

A. Free Parameters

In the B_3 mSUGRA model the boundary conditions at M_{GUT} are described by the six parameters

$$M_0, M_{1/2}, A_0, \tan\beta, \text{sgn}(\mu), \Lambda, \quad (5)$$

with

$$\Lambda \in \{\lambda_{ijk}, \lambda'_{ijk}\}. \quad (6)$$

Here M_0 , $M_{1/2}$ and A_0 are the universal scalar mass, the universal gaugino mass and the universal trilinear scalar coupling at the grand unification scale (M_{GUT}), respectively. $\tan\beta$ denotes the ratio of the Higgs vacuum expectation values (vevs) v_u and v_d , and $\text{sgn}(\mu)$ fixes the sign of the bilinear Higgs mixing parameter μ . The magnitude of μ is determined dynamically by radiative electroweak symmetry breaking (REWSB) [83]. These five parameters are the conventional free parameters of the R-parity or proton-hexality conserving mSUGRA model [84].

In order to incorporate the effects of the LNV interactions in Eq. (2) and Eq. (3) *exactly* one additional non-vanishing trilinear coupling $\Lambda \in \{\lambda_{ijk}, \lambda'_{ijk}\}$ is

assumed at M_{GUT} . Further LNV couplings are generated via the RGEs at the lower scale. Note, that the bilinear couplings κ_i and \tilde{D}_i are both set to zero at M_{GUT} via a basis transformation of the lepton and Higgs superfields [31]. (For the most general case of a complex rotation see Ref. [85].) This is natural for universal SUSY breaking [52]. However, at lower scales κ_i and \tilde{D}_i are generated via the RGEs [37]; see Sec. II C.

The complete low energy spectrum is obtained by running the RGEs down from M_{GUT} to M_{EW} . For that purpose we employ the program **SOFTSUSY-3.0.12** [86, 87]. We calculate the neutrino masses with our own program. Note that we work in the CP-conserving limit throughout this paper.

B. Benchmark Scenarios for Parameter Scans

We center our analysis around the following B_3 mSUGRA parameter points

Point I: $M_{1/2} = 500$ GeV, $M_0 = 100$ GeV, $\tan\beta = 20$, $\text{sgn}(\mu) = +1$, $A_0 = 900$ GeV, $\Lambda = \lambda'_{233}$

Point II: $M_{1/2} = 500$ GeV, $M_0 = 100$ GeV, $\tan\beta = 20$, $\text{sgn}(\mu) = +1$, $A_0 = 200$ GeV, $\Lambda = \lambda_{233}$

Point II differs from Point I only by the choice of the LNV coupling and the size of A_0 . We have chosen these points as examples because the tree-level contribution to the neutrino mass is small around Point I and II and therefore one-loop contributions are important. Both points lead to squark masses of $\mathcal{O}(1$ TeV) and slepton masses of around 300 GeV, with a scalar tau (stau) as the LSP.

Note that in the LNV SSM a stau LSP is as well motivated as a neutralino LSP [52, 58, 65, 88–90]. Either will decay via the LNV interactions and cosmological constraints do not apply [91].

In addition, we ensured that both points lie in regions of parameter space where various other experimental constraints are fulfilled, such as the lower bound on the lightest Higgs mass from LEP2 [92, 93] and constraints from the anomalous magnetic moment of the muon [94], from $b \rightarrow s\gamma$ [95], and from $B_s \rightarrow \mu^+\mu^-$ [95]; see Sec. V for details.

C. Renormalization Group Equations and Radiative Electroweak Symmetry Breaking

An important feature of the B_3 mSUGRA model is that lepton number violation leads to mixing between the lepton superfields L_i and the Higgs superfield H_d . Furthermore, sneutrinos, the superpartners of the neutrinos, can acquire vevs v_i ($i = 1, 2, 3$). Note that it is possible to rotate away the κ_i terms in the superpotential at any given energy scale by an orthogonal rotation of the fields $\mathcal{L}_\alpha \equiv (H_d, L_i)$ [31, 52, 85].

The corresponding bilinear soft-breaking terms proportional to \tilde{D}_i , Eq. (3), can be rotated away in conjunction with κ_i if \tilde{D}_i and κ_i are aligned. This condition is fulfilled at M_{GUT} in the B_3 mSUGRA model if the underlying supergravity superpotential satisfies the quite natural condition [52]

$$f(z_i; y_\alpha) = f_1(z_i) + f_2(y_\alpha), \quad (7)$$

where the superfields z_i belong to the observable sector and the superfields y_α to the hidden sector.

However, when evolving the parameters down to the weak scale, κ_i , $\tilde{D}_i \neq 0$ are generated via the RGEs. The leading terms for $\Lambda \in \{\lambda'_{ijk}\}$ are given by [52]

$$16\pi^2 \frac{d\kappa_i}{dt} = -3\kappa_i \left[\frac{g_1^2}{5} + g_2^2 - (\mathbf{Y}_U)_{33}^2 - \frac{(\mathbf{Y}_E)_{33}^2}{3} \delta_{3i} \right] - 3\mu \lambda'_{ijk} (\mathbf{Y}_D)_{jk} + \dots \quad (8)$$

and

$$16\pi^2 \frac{d\tilde{D}_i}{dt} = -3\tilde{D}_i \left[\frac{g_1^2}{5} + g_2^2 - (\mathbf{Y}_U)_{33}^2 - \frac{(\mathbf{Y}_E)_{33}^2}{3} \delta_{3i} \right] + 6\kappa_i \left[\frac{g_1^2}{5} M_1 + g_2^2 M_2 \right] + 6\kappa_i \left[(\mathbf{Y}_U)_{33} (\mathbf{h}_U)_{33} + \frac{(\mathbf{Y}_E)_{33}}{3} (\mathbf{h}_E)_{33} \delta_{3i} \right] - 3(\mathbf{Y}_D)_{jk} (2\mu h'_{ijk} + \tilde{B} \lambda'_{ijk}) + \dots \quad (9)$$

Here $t \equiv \ln(Q/\mu_0)$ with Q the renormalization scale and μ_0 an arbitrary reference scale. $h'_{ijk} \equiv A_0 \times \lambda'_{ijk}$ at M_{GUT} , *cf.* Eq. (3). \tilde{B} is the soft supersymmetry breaking analog of the Higgs mixing parameter μ and $(\mathbf{h}_U)_{33}$ [$(\mathbf{h}_E)_{33}$] is the soft-breaking analog of the Yukawa coupling $(\mathbf{Y}_U)_{33}$ [$(\mathbf{Y}_E)_{33}$] [52]. g_1 and g_2 (M_1 and M_2) are the $U(1)_Y$ and $SU(2)$ gauge couplings (gaugino masses), respectively. We see in Eqs. (8) and (9) that the RGEs differ, and therefore κ_i and \tilde{D}_i will no longer be aligned at the weak scale [37]. The case $\Lambda \in \{\lambda_{ijk}\}$ is analogous up to the color factor 3.

The sneutrino vevs v_i , the bilinear Higgs parameter $|\mu|$ and the corresponding soft breaking term \tilde{B} are determined by REWSB, which has been discussed in detail in Ref. [52] for the LNV case.

Neglecting higher order corrections [96–98], which are not important for the following qualitative discussion [116], the sneutrino vevs can be written as [52]

$$(M_\nu^2)_{ij} v_j = - \left[\mathbf{m}_{h_d \tilde{L}_i}^2 + \mu \kappa_i \right] v_d + \tilde{D}_i v_u, \quad (10)$$

with

$$(M_\nu^2)_{ij} = (\mathbf{m}_{\tilde{\mathbf{L}}}^2)_{ij} + \kappa_i \kappa_j + \frac{1}{2} M_Z^2 \cos 2\beta \delta_{ij} + \frac{(g^2 + g_2^2)}{2} \sin^2 \beta \sum_l v_l^2 \delta_{ij}, \quad (11)$$

where $(\mathbf{m}_{\tilde{\mathbf{L}}}^2)$ is the squared soft-breaking lepton doublet mass matrix and $g = \sqrt{3/5} g_1$. $\mathbf{m}_{h_d \tilde{L}_i}^2$ originates from the LNV soft-breaking Lagrangian, Eq. (3). It mixes the down-type Higgs fields, h_d , with the lepton doublet scalars, \tilde{L}_i , and is zero at M_{GUT} . That is, because we take within mSUGRA the mass matrix of the fields $\tilde{\mathcal{L}}_\alpha = (h_d, \tilde{L}_i)$ to be diagonal and proportional to M_0 at M_{GUT} . However, $\mathbf{m}_{h_d \tilde{L}_i}^2 \neq 0$ is subsequently generated via the RGEs, *cf.* Eq. (33).

As we will see in Sec. III 1, sneutrino vevs and non-zero bilinears κ_i lead to neutrino masses at tree-level because they mix neutrinos and neutralinos.

D. Quark Mixing

The RGE evolution of the parameters in the B_3 mSUGRA model from M_{GUT} to M_{EW} depends on the Higgs–Yukawa coupling matrices \mathbf{Y}_E , \mathbf{Y}_D and \mathbf{Y}_U , *cf.* Eqs. (8) and (9). In particular, the RGEs of the LNV violating parameters are coupled via the non-diagonal matrix elements of the Higgs–Yukawa couplings. Therefore a knowledge of the latter is crucial for the analysis of bounds on the LNV parameters.

The initial parameter set of the B_3 mSUGRA model at M_{GUT} is given in the electroweak basis so that for the RGE evolution the Higgs–Yukawa couplings (or the quark- and lepton-mass matrices) are also needed in the electroweak basis. However, from experiment we only know the masses and the CKM matrix

$$\mathbf{V}_{CKM} = \mathbf{U}_L^\dagger \mathbf{D}_L \quad (12)$$

at M_{EW} . Here \mathbf{U}_L^\dagger (\mathbf{D}_L^\dagger) rotate the left-handed up- (down-) quark fields from the mass eigenstate basis to the electroweak basis. For simplicity, we take \mathbf{Y}_D and \mathbf{Y}_U to be real and symmetric and thus the rotation matrices for the right-handed quark fields are identical to the ones for left-handed quark fields, $\mathbf{U}_R = \mathbf{U}_L$ and $\mathbf{D}_R = \mathbf{D}_L$. Because of the uncertainty about the neutrino masses and mixings we will assume a diagonal \mathbf{Y}_E in the weak basis.

When determining the neutrino masses, we will consider two limiting cases at M_{EW} , following Ref. [52, 58, 99]:

- “**up-type mixing**” the quark mixing is only in the up-quark sector,

$$\mathbf{U}_{L,R} = \mathbf{V}_{CKM}, \quad \mathbf{D}_{L,R} = \mathbf{1},$$

$$\mathbf{Y}_D \times v_d = \text{diag}(m_d, m_s, m_b), \quad (13)$$

$$\mathbf{Y}_U \times v_u = \mathbf{V}_{CKM} \cdot \text{diag}(m_u, m_c, m_t) \cdot \mathbf{V}_{CKM}^T.$$

- “**down-type mixing**” the mixing is only in the down-quark sector,

$$\mathbf{D}_{L,R} = \mathbf{V}_{CKM}, \quad \mathbf{U}_{L,R} = \mathbf{1},$$

$$\mathbf{Y}_D \times v_d = \mathbf{V}_{CKM} \cdot \text{diag}(m_d, m_s, m_b) \cdot \mathbf{V}_{CKM}^T,$$

$$\mathbf{Y}_U \times v_u = \text{diag}(m_u, m_c, m_t). \quad (14)$$

Here m_d, m_s, m_b (m_u, m_c, m_t) denote the masses of the down-type (up-type) quarks.

The choice between up- and down-type mixing has a strong effect on the final results for the LNV couplings $\Lambda \in \{\lambda'_{ijk}\}$ with $j \neq k$, as we will show in Sec. V (see Tab. I). The reason is that the generated tree level neutrino mass is proportional to the off-diagonal matrix element $(\mathbf{Y}_D)_{jk}^2$, cf. the discussion in Sec. III and Sec. IV. Our results (for the tree-level neutrino mass) in Sec. V can be easily translated to scenarios which lie between the limiting cases of Eqs. (13) and (14). One only needs to know the respective Yukawa matrix elements $(\mathbf{Y}_D)_{jk}$.

III. NEUTRINO MASSES

In this paper, we investigate bounds on lepton-number violating couplings at M_{GUT} within the B_3 mSUGRA model, which arise from the generation of too large neutrino masses at M_{EW} . We therefore need to identify the dominant contributions to the neutrino masses.

It was stated in Ref. [52] that the main contribution stems from mixing between neutralinos and neutrinos, which leads to one non-vanishing neutrino mass at tree-level, cf. Sec. III 1. However, as we will show in the next two sections, this is only true in parts of the B_3 mSUGRA parameter space. It is possible that the different terms in the tree-level mass formula cancel each other. We then need to identify the dominant contributions, which arise at one-loop.

A complete list of all one-loop contributions is given in Ref. [38], where they are formulated in a basis-independent manner. Most of the one-loop contributions are proportional to the mass insertions that mix the neutrinos with the neutralinos. They thus also vanish when the tree-level neutrino mass vanishes and are negligible in the region we are interested in.

The remaining dominant one-loop contributions are on the one hand due to loops involving two R-parity violating vertices and are thus either proportional to λ^2 or to λ'^2 , cf. Fig. 1 [117]. We will review these contributions in Sec. III 2. On the other hand, loops with virtual neutral scalars (*i.e.* Higgses and sneutrinos) and neutralinos, which are shown in Fig. 2, can also give large contributions to neutrino masses. These loops are proportional to the mass difference between CP-even and CP-odd sneutrinos, cf. Sec. III 3.

According to Ref. [38], there is in principle also a contribution which is proportional to $\lambda \times \tilde{D}_i$. However, this contribution is suppressed by two or more orders of magnitude in the regions of parameter space where the loops dominate over the tree-level mass. Note that \tilde{D}_i vanishes near the tree-level mass minimum as we will show in Sec. IV. We therefore neglect it in the following.

Further one-loop contributions are only present in a lepton- and Higgs-superfield basis with non-vanishing

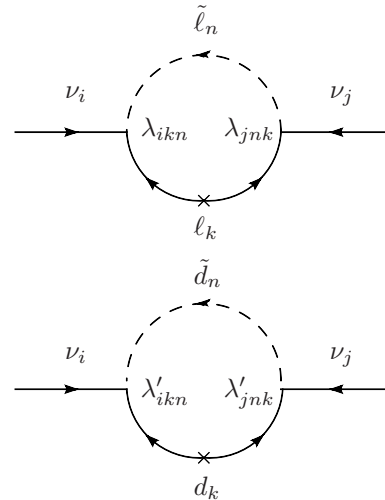


FIG. 1: Loop contributions to the neutrino mass matrix via a non-vanishing product of B_3 couplings $\lambda_{ikn} \times \lambda_{jnk}$ (upper figure) and $\lambda'_{ikn} \times \lambda'_{jnk}$ (lower figure). See Sec. III 2 for more details.

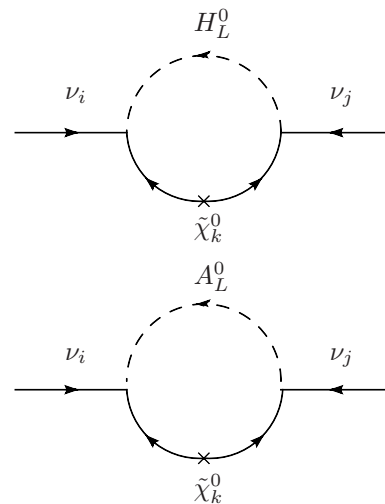


FIG. 2: Loop contributions to the neutrino mass matrix via a non-exact cancellation of loops with CP-even and CP-odd neutral scalars. Note, that there is a relative minus sign between the two diagrams. See Sec. III 3 for more details.

sneutrino vevs. This is the case in the B_3 mSUGRA model. However, we have checked that in our parameter scans, these contributions are at least one order of magnitude smaller than the dominant one and thus negligible for calculating the bounds. Note, that they are also aligned with the tree-level mass, because the sneutrino vevs vanish near the tree-level mass minimum, cf. Sec. IV A.

We conclude, that the contributions to the neutrino masses which we review in the following, are sufficient to calculate the correct bounds on the LNV couplings λ and λ' . However, in order to calculate the correct

neutrino mass spectrum and mixing angles, all one-loop contributions given in Ref. [38] must be taken into account. This lies beyond the scope of this paper.

1. Tree-Level Contributions

In the context of the B_3 mSUGRA Model, neutrino masses are generated at tree-level through mixing be-

tween neutrinos and neutralinos. Analogously to the standard see-saw mechanism [7, 16–21] (with the neutralinos taking over the role of the right-handed neutrinos), an effective 3×3 neutrino mass matrix is generated [32, 33],

$$\mathcal{M}_{\text{eff}}^\nu = \frac{\mu(M_1 g_2^2 + M_2 g^2)}{2v_u v_d (M_1 g_2^2 + M_2 g^2) - 2\mu M_1 M_2} \begin{pmatrix} \Delta_1 \Delta_1 & \Delta_1 \Delta_2 & \Delta_1 \Delta_3 \\ \Delta_2 \Delta_1 & \Delta_2 \Delta_2 & \Delta_2 \Delta_3 \\ \Delta_3 \Delta_1 & \Delta_3 \Delta_2 & \Delta_3 \Delta_3 \end{pmatrix}, \quad (15)$$

where M_1 (M_2) is the bino (wino) soft-breaking mass and

$$\Delta_i \equiv v_i - v_d \frac{\kappa_i}{\mu}, \quad i = 1, 2, 3. \quad (16)$$

This matrix has one non-zero eigenvalue which can at M_{EW} be simplified to [52]

$$m_\nu^{\text{tree}} \approx -\frac{16\pi\alpha_{\text{GUT}}}{5} \frac{\sum_{i=1}^3 \Delta_i^2}{M_{1/2}}, \quad (17)$$

if we take into account the gaugino universality assumption at M_{GUT} , leading to $M_2 = \frac{3}{5} \frac{\alpha_2^2}{\alpha_1^2} M_1 = \frac{\alpha_2^2}{\alpha_{\text{GUT}}^2} M_{1/2}$ at M_{EW} [52]. Here $\alpha_{\text{GUT}} = g_{\text{GUT}}^2/4\pi \approx 0.041$ is the grand unified gauge coupling constant [52].

2. Contributions from $\lambda\lambda$ - and $\lambda'\lambda'$ -Loops

In the region of parameter space where the tree-level neutrino mass, Eq. (17), vanishes, loop induced neutrino masses give the dominant contributions. As we will show in Sec. V, the most important loops are those proportional to the product of two LNV trilinear couplings. The corresponding squark-quark and slepton-lepton loops are shown in Fig. 1. The resulting neutrino mass contributions are [35]

$$(m_\nu^{\lambda\lambda})_{ij} = \frac{1}{32\pi^2} \sum_{k,n} \lambda_{ikn} \lambda_{jnk} m_{\ell_k} \sin 2\tilde{\phi}_n^\ell \ln \left(\frac{m_{\tilde{\ell}_{1n}}^2}{m_{\tilde{\ell}_{2n}}^2} \right) + \frac{3}{32\pi^2} \sum_{k,n} \lambda'_{ikn} \lambda'_{jnk} m_{d_k} \sin 2\tilde{\phi}_n^d \ln \left(\frac{m_{\tilde{d}_{1n}}^2}{m_{\tilde{d}_{2n}}^2} \right), \quad (18)$$

where m_{ℓ_k} (m_{d_k}) are the lepton (down-quark) masses of generation k , and $\tilde{\phi}_n^\ell$ ($\tilde{\phi}_n^d$) the mixing angles that describe the rotation of the left- and right-handed slepton (down-squark) current eigenstates of generation n

to the two mass eigenstates, $m_{\tilde{\ell}_{1n}}$ and $m_{\tilde{\ell}_{2n}}$ ($m_{\tilde{d}_{1n}}$ and $m_{\tilde{d}_{2n}}$), respectively. Note that the squared sfermion masses are linear functions of the mSUGRA parameters M_0^2 and $M_{1/2}^2$, see for example Ref. [100]. For the calculation of Eq. (18) and all following calculations, we have used the two-component spinor formalism as described in Ref. [101].

For the first two sfermion generations, the sfermion mixing angles are small and we approximate Eq. (18) by using the mass insertion approximation (MIA) as described in Ref. [41]. The slepton (and down-squark) mass eigenstates are replaced by the respective left- and right-handed eigenstates with mass $m_{\tilde{\ell}_{Ln}}$ and $m_{\tilde{\ell}_{Rn}}$. The mixing angle can be approximated by

$$\sin 2\tilde{\phi}_n^\ell = \frac{2(M_{\tilde{\ell}}^{LR})_n^2}{m_{\tilde{\ell}_{Ln}}^2 - m_{\tilde{\ell}_{Rn}}^2}, \quad (19)$$

where

$$(M_{\tilde{\ell}}^{LR})_n^2 = m_{\ell_n} \left[\frac{(\mathbf{h}_E)_{nn}}{(\mathbf{Y}_E)_{nn}} - \mu \tan \beta \right] \quad (20)$$

denotes the left-right mixing matrix element of the charged sleptons of generation n . $(\mathbf{h}_E)_{nn}$ is the trilinear soft-breaking analog of the lepton Yukawa matrix element $(\mathbf{Y}_E)_{nn}$ [52].

A similar formula is obtained for $\sin 2\tilde{\phi}_n^d$. One only needs to replace in Eq. (19) and Eq. (20) $\ell \leftrightarrow d$, $\tilde{\ell} \leftrightarrow \tilde{d}$, $(\mathbf{Y}_E)_{nn} \leftrightarrow (\mathbf{Y}_D)_{nn}$ and $(\mathbf{h}_E)_{nn} \leftrightarrow (\mathbf{h}_D)_{nn}$, where $(\mathbf{h}_D)_{nn}$ is the soft-breaking analog of the down-quark Yukawa matrix element $(\mathbf{Y}_D)_{nn}$.

3. Contributions from Neutral Scalar–Neutralino–Loops

As the final source of neutrino masses, we consider contributions arising from loops with neutral scalars and neutralinos, *cf.* Refs. [34–36]. Most important is

the contribution from sneutrino–antisneutrino mixing, as we will see in Eq. (26).

If CP is conserved, sneutrinos $\tilde{\nu}_i$ and antisneutrinos $\tilde{\nu}_i^*$ mix to form CP–invariant mass eigenstates

$$\tilde{\nu}_i^+ \equiv \frac{1}{\sqrt{2}}(\tilde{\nu}_i + \tilde{\nu}_i^*), \quad (21)$$

$$\tilde{\nu}_i^- \equiv \frac{1}{i\sqrt{2}}(\tilde{\nu}_i - \tilde{\nu}_i^*). \quad (22)$$

If lepton number is conserved, the $\tilde{\nu}_i^\pm$ masses are degenerate and the CP-even (CPE) and CP-odd (CPO) contributions to the neutrino mass from neutral scalar–neutralino–loops cancel, *cf.* Fig. 2.

In contrast, if lepton number is violated, the $\tilde{\nu}_i^\pm$ masses are in general different, so the cancellation is no longer exact. This is due to the fact that the CPE and CPO neutrinos mix differently with the CPE and CPO Higgs fields, respectively. The size of this contribution to the neutrino masses is roughly proportional to the mass splitting $\Delta m_{\tilde{\nu}_i}^2 = m_{\tilde{\nu}_i^+}^2 - m_{\tilde{\nu}_i^-}^2$, *cf.* Eq. (26) and Refs. [34–36].

The neutral scalar–neutralino–loops, shown in Fig. 2, lead to the following contributions to the neutrino mass matrix [41]

$$(m_{\tilde{\nu}}^{\tilde{\nu}\tilde{\nu}})_{ij} = \frac{1}{32\pi^2} \sum_{k=1}^4 \sum_{L=1}^5 m_{\tilde{\chi}_k^0} (gN_{1k} - g_2 N_{2k})^2 \times \left[Z_{(2+i)L}^+ Z_{(2+j)L}^+ B_0(0, m_{H_L^0}^2, m_{\tilde{\chi}_k^0}^2) - Z_{(2+i)L}^- Z_{(2+j)L}^- B_0(0, m_{A_L^0}^2, m_{\tilde{\chi}_k^0}^2) \right], \quad (23)$$

where $m_{\tilde{\chi}_k^0}$ ($k = 1 \dots 4$) are the neutralino masses and N is the 4×4 neutralino mixing matrix in the bino, wino, Higgsino basis [102]. The two-point Passarino-Veltman function is conventionally denoted B_0 [103]. $m_{H_L^0}$ ($m_{A_L^0}$) with $L = 1, \dots, 5$ are the mass eigenvalues of the CPE (CPO) neutral Higgs bosons and CPE (CPO) sneutrino fields. They can be obtained with the help of the unitary matrix Z^+ (Z^-), which diagonalizes the mass matrices of the CPE (CPO) neutral scalars, *i.e.*

$$(Z^+)^T \mathcal{M}_{\text{CPE}} Z^+ = \text{diag}(m_{h^0}^2, m_{H^0}^2, m_{\tilde{\nu}_1^+}^2, m_{\tilde{\nu}_2^+}^2, m_{\tilde{\nu}_3^+}^2) \equiv \text{diag}(m_{H_L^0}^2) \quad (24)$$

and

$$(Z^-)^T \mathcal{M}_{\text{CPO}} Z^- = \text{diag}(m_{G^0}^2, m_{A^0}^2, m_{\tilde{\nu}_1^-}^2, m_{\tilde{\nu}_2^-}^2, m_{\tilde{\nu}_3^-}^2) \equiv \text{diag}(m_{A_L^0}^2); \quad (25)$$

see Ref. [41] for additional details.

In order to analyze the dependence of this contribution on the mSUGRA parameters, we make use of the

fact that in the B_3 mSUGRA model, Eq. (23) can be approximated by [39]

$$(m_{\tilde{\nu}}^{\tilde{\nu}\tilde{\nu}})_{ij} \approx \frac{1}{32\pi^2} \sum_{k=1}^4 m_{\tilde{\chi}_k^0}^3 (gN_{1k} - g_2 N_{2k})^2 \times \frac{\Delta m_{\tilde{\nu}_i}^2}{(m_{\tilde{\nu}_i}^2 - m_{\tilde{\chi}_k^0}^2)^2} \ln \left(\frac{m_{\tilde{\chi}_k^0}^2}{m_{\tilde{\nu}_i}^2} \right) \delta_{ij} \quad (26)$$

by expanding around $m_{H_{L>2}^0}^2$ and $m_{A_{L>2}^0}^2$. The mass splitting, $\Delta m_{\tilde{\nu}_i}^2$, in Eq. (26) between CPE and CPO sneutrinos of generation i is then given by [36]

$$\Delta m_{\tilde{\nu}_i}^2 = \frac{-4\tilde{B}^2 M_Z^2 m_{\tilde{\nu}_i}^2 \sin^2 \beta}{(m_{H^0}^2 - m_{\tilde{\nu}_i}^2)(m_{h^0}^2 - m_{\tilde{\nu}_i}^2)(m_{A^0}^2 - m_{\tilde{\nu}_i}^2)} \times \frac{(\tilde{B}v_i - \tilde{D}_i v_d)^2}{(v_d^2 + v_i^2)(\tilde{B}^2 + \tilde{D}_i^2)}. \quad (27)$$

4. Numerical Implementation

The numerical calculation of the neutrino mass matrix was done in the following way. We first employed SOFTSUSY-3.0.12 [86, 87] to obtain the low energy mass spectrum [118]. We then used our own program to calculate the neutrino mass matrix. The tree-level contribution was derived from Eq. (15). For the $\lambda\lambda$ - and $\lambda'\lambda'$ -loops, we employed Eq. (18), if third generation sfermions were involved. However, for sfermions of the first two generations we used the MIA as given in Eqs. (19) and (20).

For the neutral scalar–neutralino–loops, we in principle employed Eq. (23). However, instead of performing the large numerical cancellation between CPE and CPO neutral scalars directly [square bracket in Eq. (23)], we used an MIA to calculate the deviation from exact cancellation in the R-parity conserving (RPC) limit, following Ref. [41]. The resulting formula is quite lengthy and we refer the interested reader to Ref. [41] for details. We have cross checked our program with the help of Eq. (26) and Eq. (27). All our calculations are performed in the CP-conserving limit.

IV. ν -MASSES: DEPENDENCE ON MSUGRA PARAMETERS

In the literature it has frequently been assumed that the tree-level contribution to the neutrino mass, Eq. (17), in the B_3 mSUGRA model dominates over the loop contributions, *cf.* for example Refs. [41, 52]. However, as has been noted in Ref. [54], in certain regions of B_3 mSUGRA parameter space, the tree-level neutrino mass vanishes even when $\kappa_i \neq 0$.

We demonstrate this effect in Fig. 3, where we display the tree-level neutrino mass (solid red line) as a function of A_0 . The other B_3 mSUGRA parameters are given by Point I with $\lambda'_{233}|_{\text{GUT}} = 10^{-5}$, *cf.*

Sec. II B. We see that the tree-level mass, m_ν^{tree} , vanishes around $A_0 \approx 910$ GeV. In the vicinity of this minimum, m_ν^{tree} drops by several orders of magnitude over a wide range of A_0 , and it is therefore not a (large) fine-tuning effect. In this case the loop contributions will dominate the neutrino mass matrix, resulting in much weaker bounds on the involved Λ coupling, *cf.* Sec. V. Thus the bound crucially depends on the choice of A_0 .

We emphasize that the range of A_0 for which weaker bounds may be obtained is quite large. In an interval of $\Delta A_0 \approx 100$ GeV around the minimum, we obtain bounds on λ'_{233} that are at least one order of magnitude smaller than the bound derived at for example $A_0 = 0$ GeV. Much weaker bounds can therefore be obtained without a lot of fine tuning.

In this section, we aim to explain in detail the origin of this cancellation, considering as an explicit example the case $\Lambda \in \{\lambda'_{ijk}\}$. We focus on the dependence of m_ν^{tree} on the mSUGRA parameter A_0 [for a given set of parameters $\tan\beta$, $M_{1/2}$, M_0 , and $\text{sgn}(\mu)$] such that the tree-level neutrino mass vanishes. All arguments can analogously be applied to a λ_{ijk} coupling, as discussed in App. A 5. Note for the further discussion that we can always obtain a positive Λ by absorbing a possible sign of Λ via a re-definition $L \rightarrow -L$ and $E \rightarrow -E$ of the lepton doublet and lepton singlet superfields, respectively. We also note that the generated neutrino masses scale roughly with Λ^2 , *cf.* the following discussion.

A. A_0 Dependence of the Tree-Level Neutrino Mass

We now discuss the dependence of the tree-level neutrino mass at M_{EW} as a function of A_0 at M_{GUT} . Recall from Sec. III 1 that

$$m_\nu^{\text{tree}} \propto \Delta_i^2 = \left(v_i - v_d \frac{\kappa_i}{\mu} \right)^2. \quad (28)$$

From the RGE of κ_i , Eq. (8), we obtain as the dominant contribution

$$\kappa_i \propto \mu \lambda'_{ijk} (\mathbf{Y}_D)_{jk} \equiv \mu \lambda'_{ijk} \frac{(m_d)_{jk}}{v_d} \quad (29)$$

at all energy scales, where $(m_d)_{jk}$ denotes a matrix element of the down quark mass matrix. Therefore,

$$v_d \frac{\kappa_i}{\mu} \propto \lambda'_{ijk} \cdot (m_d)_{jk}, \quad (30)$$

without further dependence on mSUGRA parameters.

Thus, the dependence of the tree-level neutrino mass, Eq. (28), on the mSUGRA parameters is solely through the sneutrino vev v_i [119]. In Fig. 3, the dashed green line explicitly shows the dependence of

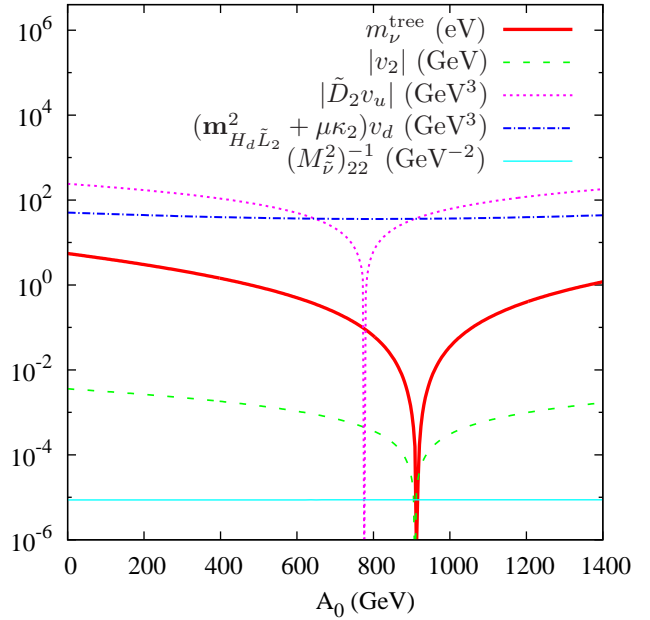


FIG. 3: A_0 dependence of m_ν^{tree} and the terms determining the sneutrino vev v_2 , Eq. (31), at the REWSB scale (used in `SOFTSUSY` to calculate the sneutrino vev). Since the scale affects the parameters only logarithmically, there are only minor changes when running to M_{EW} . The other B_3 mSUGRA parameters are that of Point I with $\lambda'_{233}|_{\text{GUT}} = 10^{-5}$, Sec. II B.

$|v_i|$, $i = 2$ on A_0 . It possesses a clear minimum which is close to the minimum of m_ν^{tree} .

This behavior can be understood by taking a look at the (tree-level) formula for the vev v_i , Eq. (10). For $\Lambda \in \{\lambda'_{ijk}\}$ it can be written as

$$v_i = \frac{1}{(M_\nu^2)_{ii}} \left[\tilde{D}_i v_u - (\mathbf{m}_{H_d \tilde{L}_i}^2 + \mu \kappa_i) v_d \right], \quad (31)$$

with

$$(M_\nu^2)_{ii} = (\mathbf{m}_{\tilde{L}}^2)_{ii} + \frac{1}{2} M_Z^2 \cos 2\beta. \quad (32)$$

Here, we have neglected terms proportional to κ_i^2 and v_i^2 , because they are much smaller than $(\mathbf{m}_{\tilde{L}}^2)_{ii}$ and M_Z^2 . Note that we only obtain one non-zero sneutrino vev because λ'_{ijk} violates only one lepton flavor.

In many regions of parameter space the sneutrino vev in Eq. (28) is at least two orders of magnitude larger than the term $v_d \kappa_i / \mu$. Thus the minimum of the neutrino mass can only occur when the sneutrino vev is drastically reduced. As we shall see, the sneutrino vev becomes very small, when there is a cancellation between the two terms in Eq. (31).

The second term of v_i in Eq. (31), $(\mathbf{m}_{H_d \tilde{L}_i}^2 + \mu \kappa_i) v_d$, and the prefactor $1/(M_\nu^2)_{ii}$ are always positive and depend only weakly on A_0 . This can be seen in Fig. 3 for $(\mathbf{m}_{H_d \tilde{L}_i}^2 + \mu \kappa_i) v_d$ (dotted-dashed blue line) and also

for $1/(M_\nu^2)_{ii}$ (solid turquoise line). This behavior can be easily understood:

The soft breaking parameter, $\mathbf{m}_{h_d \tilde{L}_i}^2$, Eq. (3), is zero at M_{GUT} and is generated at lower scales via [52]

$$16\pi^2 \frac{d\mathbf{m}_{h_d \tilde{L}_i}^2}{dt} = -\lambda'_{ijk}(\mathbf{Y}_D)_{jk} \mathcal{F}(\tilde{m}^2) - 6h'_{ijk}(\mathbf{h}_D)_{jk}, \quad (33)$$

where $\mathcal{F}(\tilde{m}^2)$ is a linear function of the soft-breaking scalar masses squared and of the down-type Higgs mass parameter squared. $h'_{ijk}[(\mathbf{h}_D)_{jk}]$ is the soft-breaking analog of $\lambda'_{ijk}[(\mathbf{Y}_D)_{jk}]$ with $h'_{ijk} = \lambda'_{ijk} \times A_0$ [$(\mathbf{h}_D)_{jk} = (\mathbf{Y}_D)_{jk} \times A_0$] at M_{GUT} . The second term in Eq. (33) thus depends on A_0^2 . However, $\mathcal{F}(\tilde{m}^2)$ is in general much larger than A_0^2 due to several contributions from soft breaking masses [52]. Therefore, varying A_0 does not significantly change the magnitude of $\mathbf{m}_{h_d \tilde{L}_i}^2$ as long as A_0 is not much larger than the sfermion masses.

Concerning the term $\mu\kappa_i$ in $(\mathbf{m}_{h_d \tilde{L}_i}^2 + \mu\kappa_i)v_d$, we note from the RGE for κ_i , Eq. (8), that the only A_0 dependence of κ_i stems from its proportionality to μ . μ at M_{EW} can be approximated by [100]

$$\mu^2 = c_1 M_0^2 + c_2 M_{1/2}^2 + c_3 A_0^2 + c_4 A_0 M_{1/2} - \frac{M_Z^2}{2}. \quad (34)$$

Here c_1 and c_2 are numbers of $\mathcal{O}(1)$ whereas c_3 and c_4 are only of $\mathcal{O}(10^{-1} - 10^{-2})$ [120]. Therefore, except for $A_0 \gg M_0, M_{1/2}$, the order of magnitude of μ remains constant when varying A_0 .

We conclude that $(\mathbf{m}_{h_d \tilde{L}_i}^2 + \mu\kappa_i)v_d$ depends only weakly on A_0 and therefore, \tilde{D}_i is decisive for the A_0 dependence of the vev v_i and thus of m_ν^{tree} . If the first term in Eq. (31), $\tilde{D}_i v_u$, is positive and only slightly larger than the (nearly constant) second term, $(\mathbf{m}_{h_d \tilde{L}_i}^2 + \mu\kappa_i)v_d$, v_i can equal $v_d \kappa_i / \mu$ and we get $m_\nu^{\text{tree}} = 0$, cf. Eq. (28).

The strong A_0 dependence of the magnitude of $\tilde{D}_i v_u$ is also displayed in Fig. 3 (dotted magenta line). We observe that $|\tilde{D}_i v_u|$ is often larger than $(\mathbf{m}_{h_d \tilde{L}_i}^2 + \mu\kappa_i)v_d$ (dotted-dashed blue line). However, near the tree-level neutrino mass minimum (solid red line), it drops below $(\mathbf{m}_{h_d \tilde{L}_i}^2 + \mu\kappa_i)v_d$ and v_i can equal $v_d \frac{\kappa_i}{\mu}$. In this case m_ν^{tree} , Eq. (28), vanishes.

In order to understand this behavior of \tilde{D}_i , we need to understand how \tilde{D}_i is generated via the RGEs. Recall that $\tilde{D}_i = 0$ at M_{GUT} within the B_3 mSUGRA model. The generation of \tilde{D}_i primarily depends on the running of the trilinear soft breaking mass h'_{ijk} [52],

$$16\pi^2 \frac{d\tilde{D}_i}{dt} = -6\mu(\mathbf{Y}_D)_{jk} h'_{ijk} + \dots \quad (35)$$

We find the contribution in Eq. (9) proportional to \tilde{B} is typically much smaller [121] and we here focus on

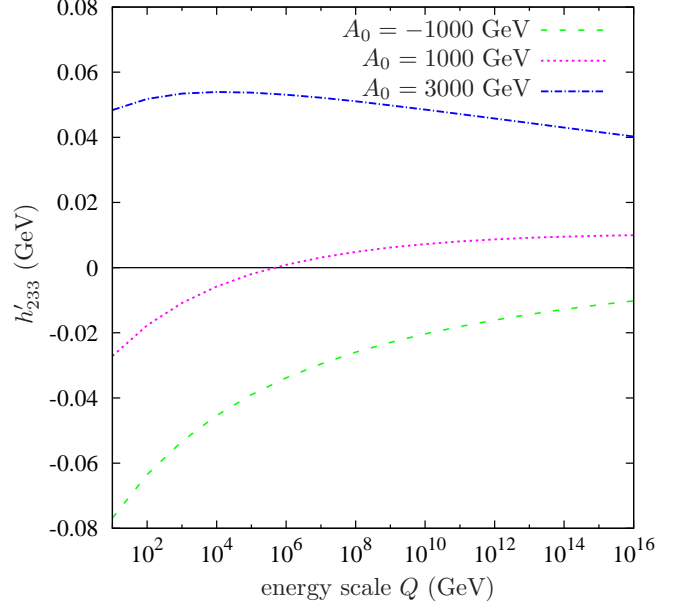


FIG. 4: Running of h'_{233} for various values of A_0 . The other B_3 mSUGRA parameters are that of Point I, Sec. II B, with $\lambda'_{233}|_{\text{GUT}} = 10^{-5}$ and $M_{1/2} = 500$ GeV.

the effects due to h'_{ijk} . The dominant terms of the corresponding RGE are given by [52, 66]

$$16\pi^2 \frac{dh'_{ijk}}{dt} = \frac{16}{3} g_3^2 (2M_3 \lambda'_{ijk} - h'_{ijk}) + \dots, \quad (36)$$

where g_3 (M_3) denotes the SU(3) gauge coupling (gaugino mass). At M_{GUT} this equation simplifies to

$$16\pi^2 \frac{dh'_{ijk}}{dt} = \frac{16}{3} g_{\text{GUT}}^2 (2M_{1/2} - A_0) \lambda'_{ijk} + \dots \quad (37)$$

Keeping for now all parameters except A_0 fixed (with $\text{sgn}(\mu) = +1$ and $\lambda'_{ijk} > 0$ [122]), we can classify the running of h'_{ijk} , Eq. (36) and Eq. (37), in the following way (see also Ref. [66] for a detailed discussion):

- (a) $A_0 \ll 2M_{1/2}$ (including negative values of A_0): Since the right hand side (RHS) of the RGE for h'_{ijk} , Eq. (36), is always positive and large, h'_{ijk} is quickly reduced from its initial value of $A_0 \times \lambda'_{ijk}$ and even becomes negative when running to lower energies. This behavior is displayed in Fig. 4 (dashed green line), where the running of h'_{233} is shown for different boundary conditions at M_{GUT} .
- (b) $A_0 \approx 2M_{1/2}$: If the size of A_0 is comparable to $2M_{1/2}$, h'_{ijk} will be fairly constant at high energies, cf. the dotted magenta line in Fig. 4. However, when running to lower energies it will still start decreasing, but more slowly than in case (a). This is due to the fact that M_3 and

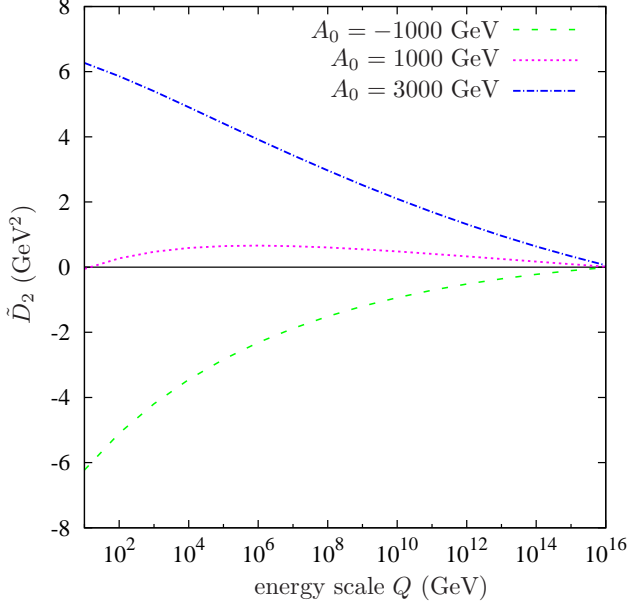


FIG. 5: Running of the bilinear coupling \tilde{D}_2 , Eq. (35), for the same parameter sets as those in Fig. 4.

λ'_{ijk} themselves increase significantly (by factors of approx. 2.5 and 3, respectively; see Ref. [66]) when running to lower energies. Thus the term $2M_3\lambda'_{ijk}$ eventually dominates in Eq. (36) even if initially $A_0 \gtrsim 2M_{1/2}$. This leads to a small, negative h'_{ijk} at low energies.

- (c) $\mathbf{A_0} \gg 2\mathbf{M_{1/2}}$: h'_{ijk} is large at M_{GUT} and is further increased when running to lower energies. This is due to the negative RHS of the RGE for h'_{ijk} , Eq. (36); see also the dotted-dashed blue line in Fig. 4.

Caveat: Since the term $2M_3\lambda'_{ijk}$ in Eq. (36) increases by a factor of approximately $8 \approx 3 \cdot 2.5$ when running from M_{GUT} to M_{EW} [as mentioned in (b)], h'_{ijk} only strictly displays the behavior of case (c) when $A_0 \gtrsim 20M_{1/2}$. Otherwise, h'_{ijk} will decrease once the term $2M_3\lambda'_{ijk}$ dominates.

Because \tilde{D}_i is zero at M_{GUT} and, according to Eq. (35), also proportional to the integral of h'_{ijk} over $\ln(Q)$, points (a) - (c) have the following consequences for \tilde{D}_i :

- (a) $\mathbf{A_0} \ll 2\mathbf{M_{1/2}}$: Since h'_{ijk} always becomes negative below some energy scale close to M_{GUT} , the RHS of Eq. (35) is positive. This leads to a large negative \tilde{D}_i at M_Z as can be seen in Fig. 5 (dashed green line). Consequently, all terms except $\tilde{D}_i v_u$ become negligible in v_i , Eq. (31), and thus $|v_i|$ at M_{EW} is large, dominating the tree-level neutrino mass, Eq. (28).

- (b) $\mathbf{A_0} \approx 2\mathbf{M_{1/2}}$: Due to the initially negative RHS

of Eq. (35) at energies close to M_{GUT} (where $h'_{ijk} \approx A_0 \times \lambda'_{ijk}$), \tilde{D}_i first increases when running to lower energies but then starts decreasing once h'_{ijk} becomes negative, *cf.* the dotted magenta lines in Fig. 4 and Fig. 5. At some energy scale Q , \tilde{D}_i becomes small such that v_i , Eq. (31), can equal $v_d \frac{\kappa_i}{\mu}$. A cancellation between these two terms in m_ν^{tree} , Eq. (28), at the scale Q will then occur. This corresponds to a vanishing tree-level neutrino mass if $Q = M_{\text{EW}}$.

- (c) $\mathbf{A_0} \gg 2\mathbf{M_{1/2}}$: The RHS of Eq. (35) is always negative with a large magnitude such that we get a large positive \tilde{D}_i at the weak scale, *cf.* the dotted-dashed blue line in Fig. 5. As in case (a), $\tilde{D}_i v_u$ provides the main contribution to $|v_i|$, Eq. (31). Therefore, $|v_i|$ is large and dominates m_ν^{tree} , Eq. (28).

Summarizing, the tree-level neutrino mass has a minimum in the parameter region where the size of A_0 is comparable to $2M_{1/2}$. This is mainly due to the running of the parameters \tilde{D}_i and h'_{ijk} that affect the sneutrino vevs; in particular due to a partial cancellation in Eq. (36). Note that in Fig. 3 the tree-level neutrino mass vanishes at $A_0 \approx 910$ GeV, which is indeed close to $2M_{1/2}$.

As we see in the following section, the position of the minimum is shifted towards higher values of A_0 for small $\tan\beta$. In this case, a change of the sign of the bilinear Higgs parameter μ also has a significant impact.

B. Dependence of the Tree-Level Neutrino Mass on the other mSUGRA Parameters

In App. A, we discuss in detail how the neutrino mass matrix depends on the other mSUGRA parameter besides A_0 . Here we summarize the most important effects and illustrate them in Fig. 6.

In Fig. 6, we show two dimensional mSUGRA parameter scans of the tree-level neutrino mass. The other mSUGRA parameters are those of Point I, Sec. II B, with $\lambda'_{233}|_{\text{GUT}} = 10^{-5}$. One scan parameter is always A_0 in order to show how the position of the minimum, which was described in the last section, changes with the other mSUGRA parameters.

Fig. 6(a) shows the A_0 - $M_{1/2}$ plane. We can clearly see that the position of the neutrino mass minimum is at $A_0 \approx 2M_{1/2}$ as was concluded above. This illustrates that varying $M_{1/2}$ has a similar effect on the running of h'_{ijk} , Eq. (36) and Eq. (37), as varying A_0 . This is clear from the arguments (a)-(c) in Sec. IV A. We could just rephrase the case differentiation as

- (a) $\mathbf{M_{1/2}} \gg \mathbf{A_0/2}$.
- (b) $\mathbf{M_{1/2}} \approx \mathbf{A_0/2}$.
- (c) $\mathbf{M_{1/2}} \ll \mathbf{A_0/2}$.

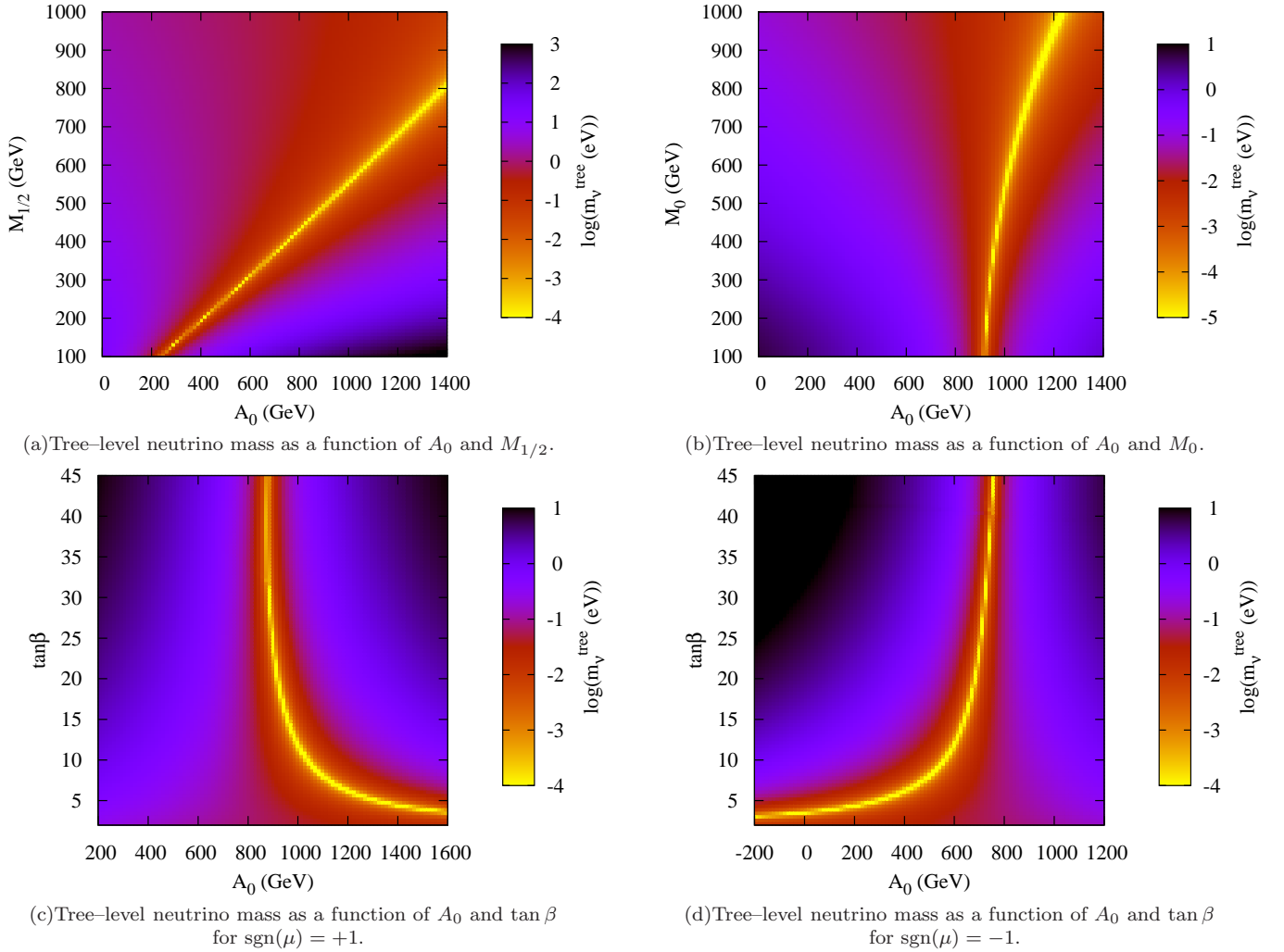


FIG. 6: Two dimensional plots of the tree-level neutrino mass. The plots are centered around parameter Point I, Sec. II B, with $\lambda'_{233}|_{\text{GUT}} = 10^{-5}$. The yellow regions signify parts of the parameter space where the neutrino mass becomes smaller than 10^{-4} eV, Figs. 6(a), 6(c), 6(d), or smaller than 10^{-5} eV, Fig. 6(b).

For $\mathbf{\Lambda} \in \{\lambda_{ijk}\}$ the relation is altered to $A_0 \approx M_{1/2}/2$. The change of the prefactor is due to the fact that λ_{ijk} couples only leptonic fields to each other. Consequently, only superfields carrying SU(2) and U(1) charges, but not SU(3) charges, contribute to the relevant RGEs; see App. A 5 for more details.

In Fig. 6(b) we present the tree-level neutrino mass as a function of A_0 and M_0 . We observe that the position of the neutrino mass minimum is fairly insensitive to M_0 , compared to A_0 , $M_{1/2}$ and $\tan\beta$ (see below). The minimum is shifted to slightly higher values of A_0 for large M_0 . However at large M_0 , the interval around the minimum in the A_0 direction where the tree-level neutrino mass is considerably reduced (and therefore the bounds on λ'_{ijk} are substantially weakened) is significantly broadened.

Finally we show in Fig. 6(c) and Fig. 6(d) the A_0 - $\tan\beta$ plane for $\text{sgn}(\mu) = +1$ and $\text{sgn}(\mu) = -1$, respectively. In Fig. 6(c) we can see that for low $\tan\beta$, the neutrino mass minimum shifts to higher values of A_0 .

This is due to a decrease of the down-type Yukawa coupling for low $\tan\beta$ leading to a decrease of the RHS of Eq. (35). This decrease needs to be balanced by increasing A_0 ; recall that $h'_{ijk} = \lambda'_{ijk} \times A_0$ at M_{GUT} in Eq. (35).

A comparison of Fig. 6(c) and Fig. 6(d) also shows that there is a *mirror effect* around $A_0 = 800$ GeV ($\approx 2M_{1/2}$) when we change the sign of the bilinear Higgs parameter μ . This happens because of a reversal of the sign of the RGE for \bar{D}_i , cf. App. A 3. Therefore the shift of the minimum for low $\tan\beta$ now appears towards *lower* values of A_0 .

C. The Dependence of the Loop Contributions to the Neutrino Mass on the mSUGRA Parameters

The loop contributions to the neutrino mass matrix are usually several orders of magnitude smaller than

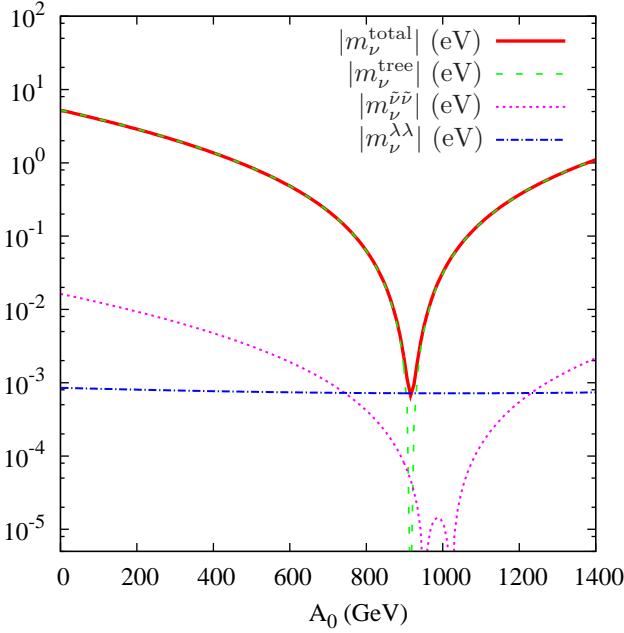


FIG. 7: A_0 dependence of the different contributions to the neutrino mass at the REWSB scale for the B_3 mSUGRA Point I, Sec. IIB, with $\lambda'_{233}|_{\text{GUT}} = 10^{-5}$. Note that only the absolute values of the contributions to the neutrino mass are displayed. m_ν^{tree} and $m_\nu^{\lambda\lambda}$ are negative whereas $m_\nu^{\tilde{\nu}\tilde{\nu}}$ is mostly positive. $m_\nu^{\tilde{\nu}\tilde{\nu}}$ is only negative between the two minima of $|m_\nu^{\tilde{\nu}\tilde{\nu}}|$; see Sec. A 6 for details.

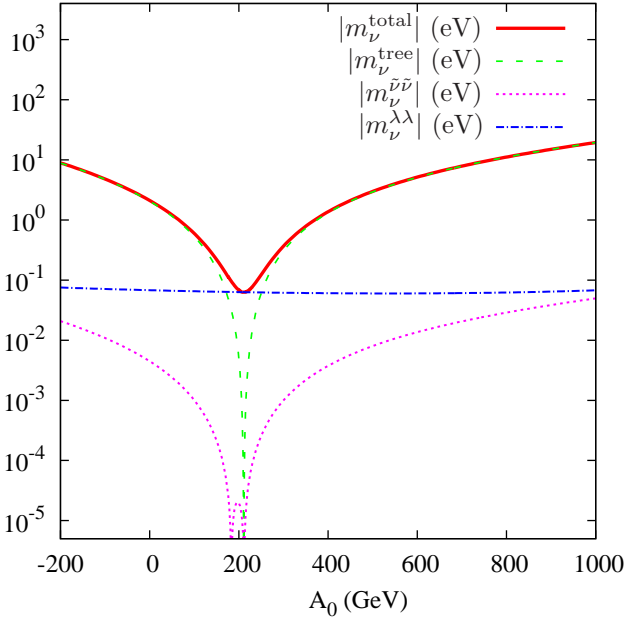


FIG. 8: Same as Fig. 7, but for the B_3 mSUGRA Point II, Sec. IIB, with $\lambda_{233}|_{\text{GUT}} = 10^{-4}$.

the tree-level contribution [41, 52]. However, in the region around the tree-level neutrino mass minimum, the loops dominate as shown in Fig. 7 and Fig. 8. Therefore, we now briefly discuss the dependence of

the loop contributions on the mSUGRA parameters.

- $\lambda\lambda$ - and $\lambda'\lambda'$ -loops: This contribution to the neutrino mass, $m_\nu^{\lambda\lambda}$, depends only weakly on the mSUGRA parameters, in particular it depends logarithmically on the relevant sfermion mass. For example, varying A_0 from 0 to 1400 GeV (−200 GeV to 1000 GeV) around Point I (Point II) leaves the magnitude of $m_\nu^{\lambda\lambda}$ nearly unchanged [123]; cf. the dotted-dashed blue line in Fig. 7 (Fig. 8). However, increasing M_0 or $M_{1/2}$ results in a decreasing $m_\nu^{\lambda\lambda}$: as the SUSY spectrum gets heavier the sfermions in the loops decouple.
- *Neutral scalar–neutralino–loops*: This contribution to the neutrino mass, $m_\nu^{\tilde{\nu}\tilde{\nu}}$, as a function of A_0 possesses a minimum which lies in the vicinity of the m_ν^{tree} minimum. However, there is no exact alignment. This behavior can be understood by noting that the minima of $m_\nu^{\tilde{\nu}\tilde{\nu}}$ arise due to the vanishing of \tilde{D}_i , because roughly

$$m_\nu^{\tilde{\nu}\tilde{\nu}} \propto \tilde{D}_i^2, \quad (38)$$

cf. App. A 6. This can be seen in Fig. 7 as well as in Fig. 8 (dotted magenta line). Again, increasing M_0 or $M_{1/2}$ will in general decrease $m_\nu^{\tilde{\nu}\tilde{\nu}}$, because the SUSY mass spectrum gets heavier.

- NLO corrections to the sneutrino vevs are typically at least one order of magnitude smaller than the tree level quantities determining the sneutrino vevs, $\mathbf{m}_{h_d \tilde{L}_i}^2 \times v_d / (M_{\tilde{\nu}})_{ii}^2$ and $\tilde{D}_i \times v_u / (M_{\tilde{\nu}})_{ii}^2$, in Eq. (10) [96]. For illustration, one could consider this as a $\mathcal{O}(10\%)$ correction to $\mathbf{m}_{h_d \tilde{L}_i}^2$. This shift upwards of the dotted-dashed blue line in Fig. 3 slightly changes the position of the tree-level neutrino mass minimum, but does not alter any of the conclusions drawn in this section. Since the effects that we investigate in this paper arise mainly from the contribution $\tilde{D}_i v_u$ to the sneutrino vevs (see Sec. IV A), these corrections are not important for the qualitative analysis.

For parameter Points I and II, Sec. IIB, the A_0 interval, ΔA_0 , where the loops dominate is relatively small, cf. Fig. 7 and Fig. 8. However, there are other parameter regions where the loops dominate in intervals of $\Delta A_0 = \mathcal{O}(100 \text{ GeV})$! This is for example the case if one varies A_0 around the benchmark point SPS1a [104]. We investigate the resulting bounds on the LNV trilinear couplings in the following section.

V. BOUNDS ON TRILINEAR B_3 COUPLINGS FROM ν -MASSES

In this section, we calculate upper bounds on all trilinear LNV couplings $\mathbf{\Lambda} \in \{\lambda_{ijk}, \lambda'_{ijk}\}$ at M_{GUT} from

the cosmological upper bound on the sum of neutrino masses as given in Eq. (4). Note that in good approximation

$$m_\nu|_{\text{EW}} \propto \Lambda^2|_{\text{GUT}}, \quad (39)$$

as explained in Sec. IV A [124], Eq. (18) and App. A 6. Based on this approximation we employ an iterative procedure to account for effects beyond Eq. (39).

In Sec. V A, we first compare our bounds with those given in Ref. [52], where the mSUGRA parameters of the benchmark point SPS1a [104] (in addition to Λ) were used. We choose the same mSUGRA parameters beside A_0 in order to show how the bounds change in the vicinity of the tree-level neutrino mass minimum, *cf.* Sec. IV A. We then perform in Sec. V C two dimensional parameter scans around the benchmark scenarios Point I and Point II (*cf.* Sec. II B) to show more generally how the bounds depend on the B_3 mSUGRA parameters.

In our parameter scans we exclude parameter regions where a tachyon occurs [52] or where the LEP2 exclusion bound on the light SSM Higgs mass is not fulfilled [92, 93]. However, we reduce the LEP2 bound by 3 GeV in order to account for numerical uncertainties of **SOFTSUSY** [105–107]. For instance, in the decoupling limit (where the light Higgs, h^0 , is SM-like) a lower bound of

$$m_{h^0} > 111.4 \text{ GeV} \quad (40)$$

is imposed. In the figures, we also show contour lines for the 2σ window of the SUSY contribution to the anomalous magnetic moment of the muon [94, 108–110]

$$8.6 \times 10^{-10} < \delta a_\mu^{\text{SUSY}} < 40.6 \times 10^{-10}. \quad (41)$$

For more details see Ref. [66] and references therein.

We also note that the complete parameter space which we investigate in the following (having rejected parameter regions which contain tachyons or violate the LEP2 Higgs bound) is consistent with the experimental upper bound on the branching ratio of $B_s \rightarrow \mu^+ \mu^-$ [95], *i.e.*

$$\text{BR}(B_s \rightarrow \mu^+ \mu^-) < 4.7 \times 10^{-8}, \quad (42)$$

and with the 2σ window for the branching ratio of $b \rightarrow s\gamma$, [95, 111],

$$2.74 \times 10^{-4} < \text{BR}(b \rightarrow s\gamma) < 4.30 \times 10^{-4}. \quad (43)$$

We employed **micrOMEGAS2.2** [112], for the evaluation of $\delta a_\mu^{\text{SUSY}}$, $\text{BR}(B_s \rightarrow \mu^+ \mu^-)$, and $\text{BR}(b \rightarrow s\gamma)$. Note that there is a significant correlation in mSUGRA models between the muon anomalous magnetic moment and $B_s \rightarrow \mu^+ \mu^-$ [113]. Furthermore, we are well above the standard supersymmetric mass bounds, as for example on the charginos.

A. Comparison with Previous Results

In Ref. [52], bounds on single couplings Λ at M_{GUT} in the B_3 mSUGRA model were determined for the mSUGRA parameters of SPS1a, in particular $A_0 = -100$ GeV. However, the possibility of obtaining much weaker bounds on the coupling Λ in the region of the tree-level neutrino mass minimum was not exploited. Note that the bounds in Ref. [52] were also obtained for a less restrictive cosmological bound of $\sum m_{\nu_i} < 0.71$ eV [125]. We present here an update of these results by using Eq. (4). We then explore the mSUGRA parameter dependence of the bounds.

In Tab. I and Tab. II ($\Lambda \in \{\lambda'_{ijk}\}$ and $\Lambda \in \{\lambda_{ijk}\}$, respectively), we compare the previous results with bounds (at M_{GUT}) that we obtain for identical B_3 mSUGRA parameter points, where only the choice of A_0 differs. In order to obtain corresponding bounds at M_{EW} one needs to take into account the RGE evolution of the couplings. Quantitatively this results in multiplying the bounds in Tab. I (Tab. II) by roughly a factor of 3.5 (1.5), *cf.* Ref. [44, 52, 54, 58, 67].

In addition to $A_0 = -100$ GeV (SPS1a), we choose two parameter points which lie $\Delta A_0 \approx 10$ GeV and $\Delta A_0 \approx 60 - 70$ GeV, away from the neutrino mass minimum. In Tab. I ($\Lambda \in \{\lambda'_{ijk}\}$), we choose $A_0 = 500$ GeV (column 3 and 6) and $A_0 = 550$ GeV (column 4 and 7). In Tab. II ($\Lambda \in \{\lambda_{ijk}\}$), we choose $A_0 = 200$ GeV (column 3) and $A_0 = 120$ GeV (column 4). This enables us to examine the dependence of the bounds on A_0 around the tree-level mass minimum.

Note that at SPS1a and when varying A_0 , the neutrino mass minimum for $\lambda'_{ijk} \neq 0$ lies at $A_0 = 563$ GeV. This value is mostly independent of the choice of the indices i, j, k . This is clear because the condition for the minimum to occur, $A_0 \approx 2M_{1/2}$, does not depend on i, j, k , *cf.* Sec. IV. Similarly, for $\lambda_{ijk}|_{\text{GUT}} \neq 0$ the minimum is expected at $A_0 \approx M_{1/2}/2$. For the SPS1a parameters we thus obtain $A_0 \approx 127$ GeV [126].

We first concentrate on Tab. I. Comparing the columns for $A_0 = -100$ GeV and then for $A_0 = 500$ GeV, *i.e.* approaching the minimum up to $\Delta A_0 = 63$ GeV, the bounds from too large neutrino masses are weakened by a factor of 13–15. When we go even closer, *i.e.* $A_0 = 550$ GeV and $\Delta A_0 = 13$ GeV, the bounds are weakened by a factor of 40–64 compared to $A_0 = -100$ GeV. As we discuss below, in the case of up-mixing, some couplings in Tab. I (column 2–4) can not be restricted at all by too large neutrino masses. In this case we show the bounds at M_{GUT} [marked by $()^t$], that one obtains from the absence of tachyons; see also Ref. [52].

We differentiate in Tab. I between up- and down-type quark mixing, *cf.* Sec. II D. Different quark mixing has important consequences for the bounds on the couplings λ'_{ijk} if $j \neq k$. As is clear from Sec. (IV A), the tree-level neutrino mass is generated proportional to $\lambda'_{ijk} \times (\mathbf{Y}_D)_{jk}$. Thus, no tree-level mass is gener-

	Up mixing			Down mixing		
A_0 (GeV)	-100	500	550	-100	500	550
λ'_{111}	2.0×10^{-3}	2.7×10^{-2}	8.3×10^{-2}	9.7×10^{-4}	1.3×10^{-2}	5.3×10^{-2}
λ'_{211}	2.0×10^{-3}	2.7×10^{-2}	8.3×10^{-2}	9.7×10^{-4}	1.4×10^{-2}	5.3×10^{-2}
λ'_{311}	2.0×10^{-3}	2.7×10^{-2}	8.3×10^{-2}	9.6×10^{-4}	1.3×10^{-2}	5.3×10^{-2}
$\lambda'_{121}, \lambda'_{112}$	$(1.3 \times 10^{-1})^t$	$(1.7 \times 10^{-1})^t$	$(1.7 \times 10^{-1})^t$	4.3×10^{-4}	6.0×10^{-3}	2.7×10^{-2}
$\lambda'_{221}, \lambda'_{212}$	$(1.3 \times 10^{-1})^t$	$(1.7 \times 10^{-1})^t$	$(1.7 \times 10^{-1})^t$	4.3×10^{-4}	6.0×10^{-3}	2.7×10^{-2}
$\lambda'_{321}, \lambda'_{312}$	$(1.3 \times 10^{-1})^t$	$(1.7 \times 10^{-1})^t$	$(1.7 \times 10^{-1})^t$	4.3×10^{-4}	5.9×10^{-3}	2.6×10^{-2}
λ'_{131}	$(1.4 \times 10^{-1})^t$	$(1.9 \times 10^{-1})^t$	$(1.9 \times 10^{-1})^t$	6.9×10^{-4}	9.5×10^{-3}	4.2×10^{-2}
λ'_{231}	$(1.4 \times 10^{-1})^t$	$(1.9 \times 10^{-1})^t$	$(1.9 \times 10^{-1})^t$	6.9×10^{-4}	9.5×10^{-3}	4.3×10^{-2}
λ'_{331}	$(1.4 \times 10^{-1})^t$	$(1.9 \times 10^{-1})^t$	$(1.9 \times 10^{-1})^t$	6.8×10^{-4}	9.3×10^{-3}	4.2×10^{-2}
λ'_{122}	9.1×10^{-5}	1.3×10^{-3}	5.3×10^{-3}	8.9×10^{-5}	1.2×10^{-3}	5.2×10^{-3}
λ'_{222}	9.1×10^{-5}	1.3×10^{-3}	5.3×10^{-3}	8.9×10^{-5}	1.2×10^{-3}	5.2×10^{-3}
λ'_{322}	9.0×10^{-5}	1.3×10^{-3}	5.3×10^{-3}	8.8×10^{-5}	1.2×10^{-3}	5.2×10^{-3}
λ'_{132}	2.4×10^{-2}	$(1.9 \times 10^{-1})^t$	$(1.9 \times 10^{-1})^t$	5.8×10^{-5}	8.0×10^{-4}	3.9×10^{-3}
λ'_{232}	2.4×10^{-2}	$(1.9 \times 10^{-1})^t$	$(1.9 \times 10^{-1})^t$	5.8×10^{-5}	8.0×10^{-4}	3.9×10^{-3}
λ'_{332}	2.4×10^{-2}	$(1.9 \times 10^{-1})^t$	$(1.9 \times 10^{-1})^t$	5.8×10^{-5}	7.9×10^{-4}	3.8×10^{-3}
λ'_{113}	4.2×10^{-3}	5.5×10^{-2}	1.9×10^{-1}	6.3×10^{-4}	8.7×10^{-3}	3.8×10^{-2}
λ'_{213}	4.2×10^{-3}	5.5×10^{-2}	1.9×10^{-1}	6.3×10^{-4}	8.7×10^{-3}	3.8×10^{-2}
λ'_{313}	4.2×10^{-3}	5.4×10^{-2}	1.7×10^{-1}	6.2×10^{-4}	8.6×10^{-3}	3.7×10^{-2}
λ'_{123}	5.9×10^{-4}	8.7×10^{-3}	2.4×10^{-2}	5.3×10^{-5}	7.4×10^{-4}	3.4×10^{-3}
λ'_{223}	5.9×10^{-4}	8.7×10^{-3}	2.4×10^{-2}	5.3×10^{-5}	7.4×10^{-4}	3.4×10^{-3}
λ'_{323}	5.8×10^{-4}	8.5×10^{-3}	2.4×10^{-2}	5.3×10^{-5}	7.2×10^{-4}	3.4×10^{-3}
λ'_{133}	2.3×10^{-6}	3.2×10^{-5}	1.3×10^{-4}	2.3×10^{-6}	3.2×10^{-5}	1.3×10^{-4}
λ'_{233}	2.3×10^{-6}	3.2×10^{-5}	1.3×10^{-4}	2.3×10^{-6}	3.2×10^{-5}	1.3×10^{-4}
λ'_{333}	2.3×10^{-6}	3.1×10^{-5}	1.3×10^{-4}	2.3×10^{-6}	3.1×10^{-5}	1.3×10^{-4}

TABLE I: Upper bounds on the trilinear couplings λ'_{ijk} , Eq. (2), at M_{GUT} for several values of A_0 (second row). The other mSUGRA parameters are those of SPS1a [104]. We assume up-mixing (down-mixing) in column 2-4 (5-7), *cf.* Sec. IID. Bounds arising from the absence of tachyons are in parentheses and marked by a superscript t : $()^t$.

A_0 (GeV)	-100	200	120
λ_{211}	1.1×10^{-1}	2.7×10^{-1}	$(7.1 \times 10^{-1})^t$
λ_{311}	1.1×10^{-1}	2.7×10^{-1}	$(7.1 \times 10^{-1})^t$
λ_{231}	$(5.5 \times 10^{-1})^t$	$(6.7 \times 10^{-1})^t$	$(7.1 \times 10^{-1})^t$
λ_{122}	4.7×10^{-4}	1.7×10^{-3}	4.9×10^{-3}
λ_{322}	4.7×10^{-4}	1.7×10^{-3}	4.9×10^{-3}
λ_{132}	$(5.5 \times 10^{-1})^t$	$(6.7 \times 10^{-1})^t$	$(7.1 \times 10^{-1})^t$
λ_{123}	$(5.1 \times 10^{-1})^t$	$(6.3 \times 10^{-1})^t$	$(6.7 \times 10^{-1})^t$
λ_{133}	2.7×10^{-5}	1.0×10^{-4}	2.8×10^{-4}
λ_{233}	2.7×10^{-5}	1.0×10^{-4}	2.8×10^{-4}

TABLE II: Upper bounds on the trilinear couplings λ_{ijk} , at M_{GUT} for different values of A_0 (first row). The other mSUGRA parameters are those of SPS1a [104]. Bounds arising from the absence of tachyons are marked by $()^t$.

ated at this level when we consider $j \neq k$ and up-type mixing (which implies a diagonal \mathbf{Y}_D). But, an additional λ'_{ikk} coupling will be generated via RGE running at lower scales, *cf.* Ref. [52]. This coupling will still generate a tree-level neutrino mass, which is however suppressed by the additional one-loop effect [127].

This effect can be seen in Tab. I, if we compare for example the upper bounds on λ'_{223} and λ'_{233} for up-

and down-type quark mixing. The ratio between these bounds is roughly 200 in the case of up-type mixing whereas there is only one order of magnitude difference for down-type mixing.

In the latter case, the ratio between the λ'_{223} and

λ'_{233} bounds originates mainly from the ratio

$$\frac{(\mathbf{Y}_D)_{23}}{(\mathbf{Y}_D)_{33}} = \frac{(\mathbf{V}_{CKM})_{23}}{(\mathbf{V}_{CKM})_{33}}, \quad (44)$$

since the tree-level mass is generated via $\lambda'_{223} \times (\mathbf{Y}_D)_{23}$ and $\lambda'_{233} \times (\mathbf{Y}_D)_{33}$, respectively.

To conclude, the bounds from the generation of neutrino masses (at least in the case of down-type mixing) are usually the strongest bounds on the couplings λ'_{ijk} at M_{GUT} . As considered in Ref. [52], they range from $\mathcal{O}(10^{-4})$ to $\mathcal{O}(10^{-6})$ for the parameter point SPS1a (column 5 in Tab. I). However, there is a large window around the tree-level neutrino mass minimum, where bounds may be obtained that are between one and two orders of magnitude weaker than those in Ref. [52]. Around the minimum, the couplings are only bounded from above by $\mathcal{O}(10^{-2})$ to $\mathcal{O}(10^{-4})$ (*cf.* column 7 in Tab. I). Thus, other low energy bounds become competitive [44, 51, 114].

We now discuss in Tab. II the case of a non-vanishing coupling λ_{ijk} at M_{GUT} . Contrary to Tab. I, in the case considered in Tab. II the quark mixing assumption does not affect the bounds since λ_{ijk} couples only to lepton superfields. Due to the antisymmetry $\lambda_{ijk} = -\lambda_{jik}$ there are only 9 independent couplings.

We observe in Tab. II that if $i \neq j \neq k \neq i$ there are no bounds from too large neutrino masses. The only bound we obtain stems from the absence of tachyons. This is because we assume a diagonal lepton Yukawa matrix \mathbf{Y}_E as stated in Sec. II D and therefore, only couplings of the form λ_{ikk} can generate a neutrino mass [128].

For these couplings, the bounds at M_{GUT} for $A_0 = -100$ GeV (column 2) range from 1.1×10^{-1} (λ_{211} and λ_{311}) to 2.7×10^{-5} (λ_{133} and λ_{233}). If we approach the tree-level mass minimum, *i.e.* going from column 2 to column 4 with $A_0 = 120$ GeV, the bound is weaker than the tachyon bound (λ_{211} and λ_{311}) or it is weakened to 2.8×10^{-4} (λ_{133} and λ_{233}). The bounds from neutrino masses are thus decreased by roughly a factor of 10.

Comparing the bounds on λ_{ikk} at M_{GUT} , one can see nicely how the choice of k influences the strength of the bound. The bounds resemble the hierarchy between the lepton Yukawa couplings $(\mathbf{Y}_E)_{kk}$ analogously to Eq. (44). Therefore, the bounds are strongest for $k = 3$.

In contrast to Tab. I, the bounds are only reduced by one order of magnitude when we approach the tree-level mass minimum. This is because the loop contributions play an important role for the bounds in Tab. II, as we discuss in the following section.

B. Influence of Loop Contributions

We now shortly discuss the influence of the neutrino mass loop contributions on the bounds. Typically, one

expects that the closer we approach the tree-level neutrino mass minimum the more important the loop contributions become. This is because the loops are not aligned to the tree-level mass, *cf.* Sec. IV C.

However, in the case of the neutral scalar loops there is still partial alignment, because both the tree-level mass minimum and the minima of the neutral scalar loops crucially depend on the vanishing of the bilinear LNV parameter \tilde{D}_i , *cf.* Sect. IV C. Therefore, it is the $\lambda'\lambda'$ -loops and $\lambda\lambda$ -loops, Sec. III 2, that are relevant whenever the loop contributions become dominant over the tree-level contributions.

We now give a few examples. For $\mathbf{\Lambda} \in \{\lambda_{ijk}\}$, Tab. II, the loop contributions dominate over the tree-level mass in a range of $\Delta A_0 \approx \pm 50$ GeV around the tree-level mass minimum at $A_0 = 127$ GeV. Therefore, the bounds in this region are much more restrictive (*i.e.* the value of the bounds *decreases*) when taking into account the loop contributions. For example,

$$\frac{\lambda_{233}^{\text{tot}}}{\lambda_{233}^{\text{tree}}} \approx 0.3, \quad (45)$$

for $A_0 = 120$ GeV; column 4 in Tab. II. Here, $\lambda_{233}^{\text{tot}}$ is the bound on λ_{233} at M_{GUT} if we take into account both tree-level and loop-contributions to the neutrino mass. In contrast, $\lambda_{233}^{\text{tree}}$ would be the bound if we only employ the tree-level mass.

Further away from the minimum, the influence of the loop contributions is weaker. The bounds are strengthened by approximately 5% for $A_0 = 200$ GeV (column 3 of Tab. II) and $< 1\%$ for $A_0 = -100$ GeV (column 2 of Tab. II).

The loop contributions are less important for the bounds in Tab. I, *i.e.* $\mathbf{\Lambda} \in \{\lambda'_{ijk}\}$. For example, even near the tree-level mass minimum (column 4 and 7 with $A_0 = 550$ GeV), the bounds become only stronger by up to 20% if we take the loop induced neutrino masses in addition to the tree-level mass into account.

C. Dependence of Bounds on \mathbf{B}_3 mSUGRA Parameters

In this section, we discuss the dependence of the bounds on $\mathbf{\Lambda} \in \{\lambda_{ijk}, \lambda'_{ijk}\}$ at M_{GUT} on the \mathbf{B}_3 mSUGRA parameters. For that purpose we perform two-dimensional parameter scans around the benchmark scenarios, Point I and Point II, of Sec. II B. For the calculation of the bounds all contributions to the neutrino mass considered in Sec. III are included. We will focus here on the couplings λ'_{233} and λ_{233} , because these couplings have the strongest constraints from neutrino masses, *cf.* Tab. I and Tab. II.

We have analyzed in Sec. IV how the neutrino mass changes with the mSUGRA parameters. Due to its approximate proportionality to $\mathbf{\Lambda}^2$, *cf.* Eq. (39), the analysis in Sec. IV is directly transferable to the mSUGRA dependence of bounds on the LNV trilinear

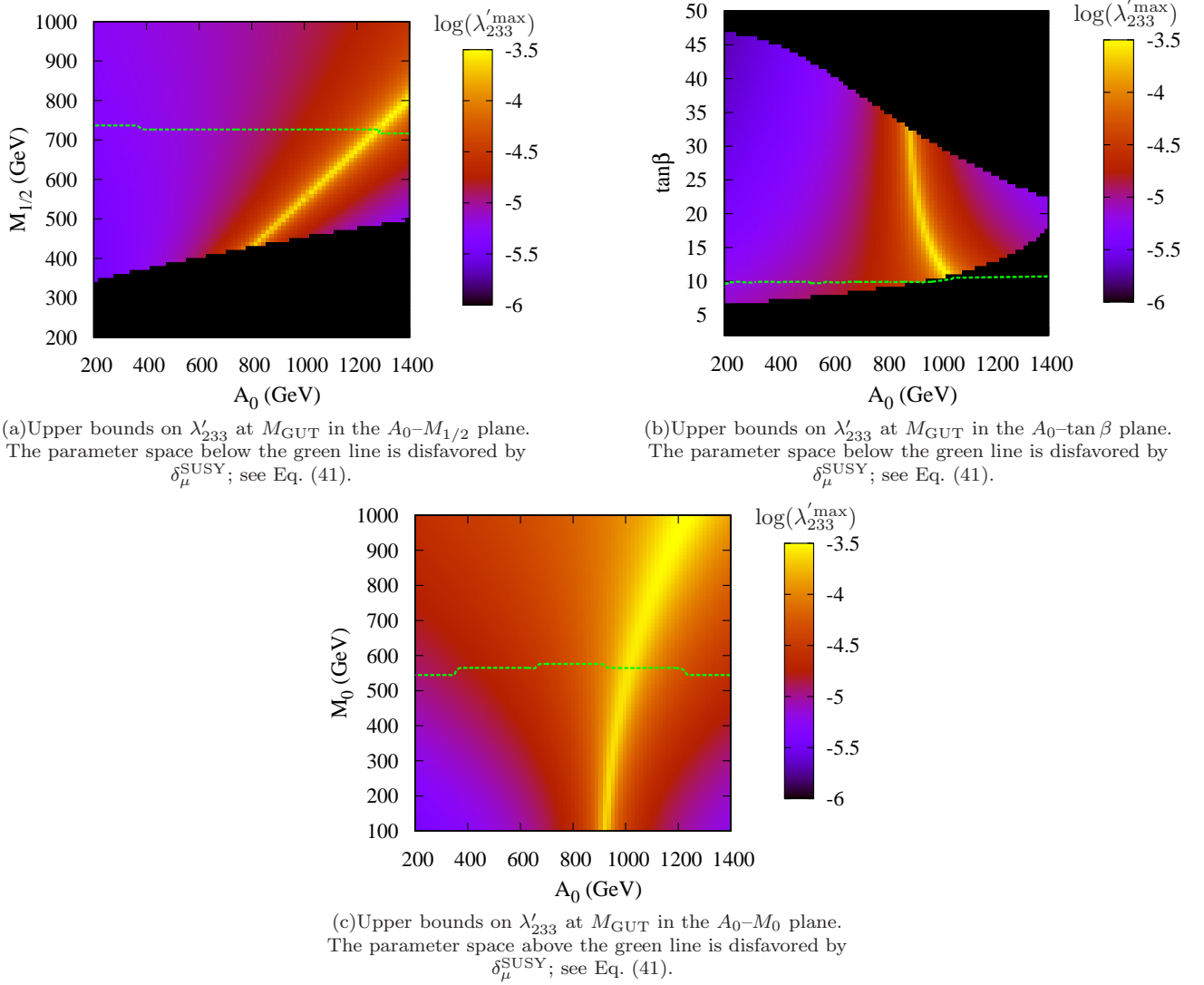


FIG. 9: Upper bounds on λ'_{233} at M_{GUT} from the cosmological bound on the sum of neutrino masses, Eq. (4), as a function of mSUGRA parameters. The parameter scans are centered around the benchmark Point I, *cf.* Sec. II B. The blackened-out region denotes parameter points where tachyons occur or where the LEP2 Higgs bound is violated.

couplings. Therefore, the parameter scans presented in this section, *i.e.* Fig. 9 and Fig. 10, resemble closely those in Fig. 6, Sec. IV.

We show in Fig. 9 [Fig. 10] how the bounds on λ'_{233} [λ_{233}] at M_{GUT} vary with mSUGRA parameters. We present in Figs. 9(a)–9(c) [Figs. 10(a)–10(c)] the A_0 – $M_{1/2}$, A_0 – $\tan \beta$, and A_0 – M_0 planes, respectively. The bounds are shown on a logarithmic scale. The blackened out regions designate areas of parameter space which are rejected due to tachyons in the model or violation of the LEP2 bound on the lightest Higgs mass, *cf.* Eq. (40). Furthermore, we include contour lines of the 2σ window for the SUSY contribution to the anomalous magnetic moment of the muon, Eq. (41). Imposing Eq. (41) disfavors the parameter space below [above] the green contour line in Figs. 9(a), 9(b), 10(a), and 10(b) [Fig. 9(c) and Fig. 9(c)].

We observe in Fig. 9 that the strictest bounds on

λ'_{233} from too large neutrino masses are of $\mathcal{O}(10^{-6})$. However, there are sizable regions of parameter space where the bounds are considerably weakened. For example, in the A_0 – $M_{1/2}$ plane, Fig. 9(a), the bounds are of $\mathcal{O}(10^{-6})$ only in approximately half of the parameter space whereas in the other half, the bounds are $\mathcal{O}(10^{-5})$ or weaker. In roughly 10% of the allowed region in Fig. 9, the bounds even lie at or above $\mathcal{O}(10^{-4})$! In this region, the loop contributions to the heaviest neutrino mass are essential for determining the bounds since the corresponding tree-level neutrino mass vanishes, *cf.* also the discussion in Sec. V B.

We can see in Fig. 10 a similar behavior for the parameter dependence of the bounds on λ_{233} . Here, the strongest bounds are now of $\mathcal{O}(10^{-5})$. However, for example in the A_0 – M_0 plane, Fig. 10(c), the bounds are as strong as $\mathcal{O}(10^{-5})$ in only about 25% of the

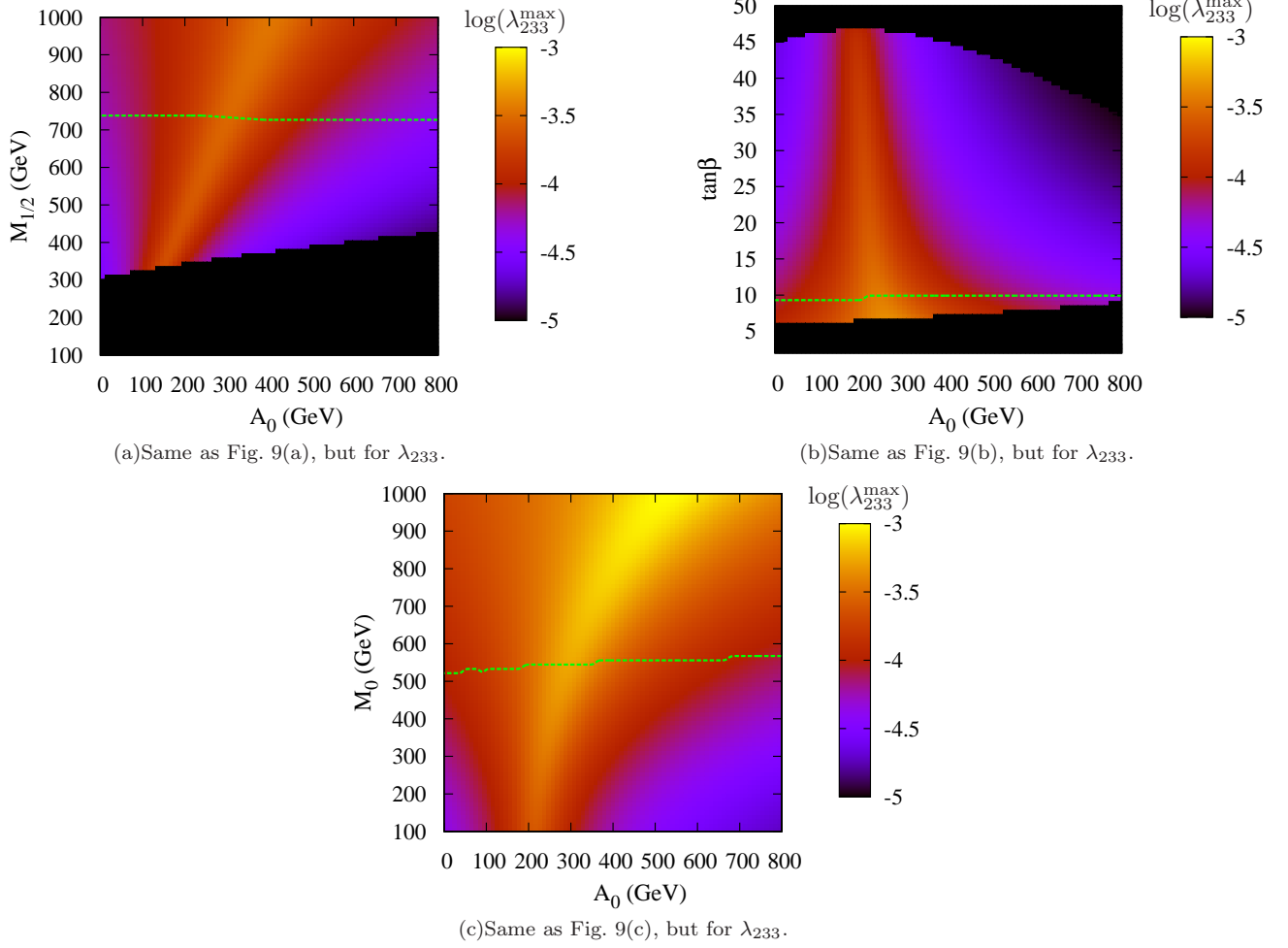


FIG. 10: Same as Fig. 9, but for λ'_{233} at M_{GUT} and for the benchmark scenario Point II, *cf.* Sec. II B.

parameter plane. The remaining 75% have bounds of $\mathcal{O}(10^{-4})$ (50%) or even $\mathcal{O}(10^{-3})$ (25%)!

Up to now, we have analyzed how the bounds on the trilinear LNV couplings λ'_{233} and λ_{233} vary with the mSUGRA parameters. However, from the analysis in Sec. V A, we can easily deduce how most of these bounds change for different couplings λ'_{ijk} and λ_{ijk} , *i.e.* for different indices i, j, k . For λ'_{ijk} the index i does not significantly influence the bound, because the employed Yukawa coupling, $(\mathbf{Y}_D)_{jk}$, via which the tree-level mass is generated, does not depend on i . But, the situation is totally different when we change the indices j, k . In general, for λ'_{ijk} (and down-mixing) the bounds will display the hierarchy of the down-type Yukawa couplings. Therefore, bounds for couplings λ'_{i11} are about three orders of magnitude weaker than bounds for the couplings λ'_{i33} as long as the other B_3 mSUGRA parameter are the same. We also observe a similar behavior for λ'_{ijk} with up-mixing and for λ_{ijk} [using $(\mathbf{Y}_E)_{jk}$ instead of $(\mathbf{Y}_D)_{jk}$], if $j = k$; *cf.* the discussion in Sec. V A.

To conclude, one can use the Yukawa matrix \mathbf{Y}_D (\mathbf{Y}_E) to easily translate the bounds in Fig. 9 (Fig. 10)

to bounds on couplings other than λ'_{233} (λ_{233}).

VI. SUMMARY AND CONCLUSION

We have calculated upper bounds on all trilinear lepton number violating couplings at the grand unification scale within the B_3 (*i.e.* lepton number violating) minimal supergravity (mSUGRA) model, which result from the cosmological bound on the sum of neutrino masses. We have shown that these bounds on the couplings can be weaker by one to two orders of magnitude compared to the ones which were previously presented in the literature for the benchmark scenario SPS1a; *cf.* Sec. V. In general, the bounds can be as weak as $\mathcal{O}(10^{-1})$. Thus other low energy bounds become competitive.

The reason for these large effects is that the tree-level neutrino mass depends strongly on the trilinear soft-breaking A_0 -parameter (and also similarly on the gaugino masses). We concluded in Sec. IV, that in regions of parameter space with $A_0 \approx 2M_{1/2}$ ($A_0 \approx M_{1/2}/2$) for $\lambda'_{ijk}|_{\text{GUT}} \neq 0$ ($\lambda_{ijk}|_{\text{GUT}} \neq 0$), a

cancellation between the different contributions to the tree-level mass can occur. We have explained this effect in detail and have shown that such a cancellation is significant in large regions of the mSUGRA parameter space. For example, the bounds can be weakened by one order of magnitude in A_0 intervals of up to $\mathcal{O}(100 \text{ GeV})$, see Figs. 9 and 10. Therefore, much weaker bounds (compared to previous ones) can be obtained without significant fine-tuning.

In order to obtain the correct bounds in the vicinity of the tree-level neutrino mass minimum, we included the main loop contributions to the neutrino mass matrix; *cf.* Sec. III. We also described in Sec. IV and App. A for the first time the dependence of the tree-level *and* loop induced neutrino mass on all mSUGRA parameters. Although we concentrated in this work on the B₃ mSUGRA model, the mechanisms described will also work in more general R-parity violating models.

Our work can help to find new supersymmetric scenarios that are consistent with the observed neutrino masses and mixings. We have shown in this publication how the (typically large) hierarchy between the tree-level and 1-loop neutrino masses can systematically be reduced. Together with at least one additional lepton number violating coupling, one can use this mechanism to match the ratio between tree-level and 1-loop induced masses to the observed neutrino mass hierarchy, both for hierarchical neutrino masses and for a degenerate spectrum.

We also note, as described in the introduction, that large lepton number violating couplings can lead to distinct collider signatures. We will address these topics in future publications.

Acknowledgments

We thank Ben Allanach, Howie Haber, Jong Soo Kim and Steve C. H. Kom for discussions. The work of H. Dreiner was partially financed by the SFB-TR 33 ‘The Dark Universe’ and partially by DOE grant DE-FG02-04ER41286. S. Grab’s work was financed by the DOE grant DE-FG02-04ER41286. The work of M. Hanussek was funded by the Konrad-Adenauer-Stiftung, the Bonn Cologne Graduate School and the Deutsche Telekom Stiftung.

Appendix A: ν -Masses: Dependence on Further B₃ mSUGRA Parameters

In Sec. IV A, we described in detail the dependence of the tree-level neutrino mass, Eq. (17), on the B₃ mSUGRA parameter A_0 . We also reviewed some further effects in Sec. IV B. In this appendix, we explain now in more detail the dependence of the tree-level neutrino mass and the loop induced masses on the remaining B₃ mSUGRA parameters.

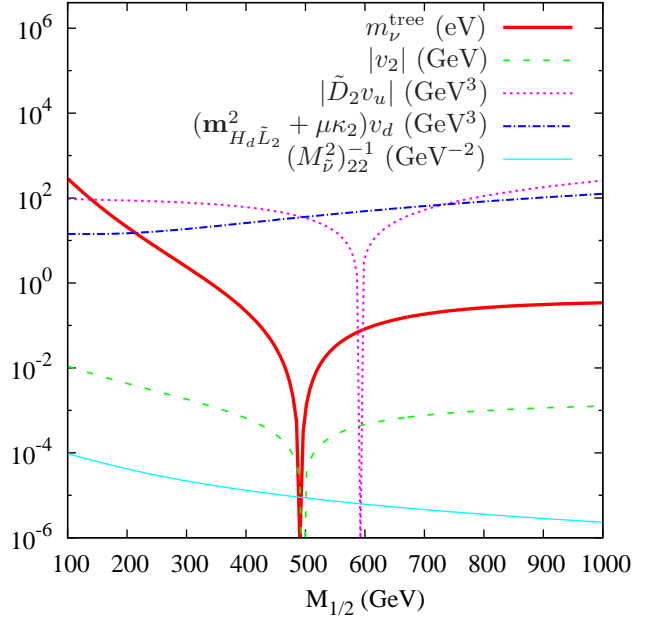


FIG. 11: Same as Fig. 3, but now for the mSUGRA parameter $M_{1/2}$ instead of A_0 .

1. $M_{1/2}$ Dependence

The tree-level neutrino mass minimum can be explained equivalently in terms of its dependence on $M_{1/2}$ instead of its dependence on A_0 . This is because varying $M_{1/2}$ has a similar effect on the sneutrino vev v_i , Eq. (31), as varying A_0 , *cf.* Sec. IV A and Sec. IV B. However, when varying $M_{1/2}$ there are *additional effects* coming on the one hand from the dependence of μ^2 , $(M_{\tilde{\nu}}^2)_{ii}$ and $\mathbf{m}_{H_d \tilde{L}_i}^2$ on $M_{1/2}$. These quantities are linear functions of $M_{1/2}^2$. For μ^2 this can be seen from Eq. (34). For $(M_{\tilde{\nu}}^2)_{ii}$ and $\mathbf{m}_{H_d \tilde{L}_i}^2$ this follows because the respective RGEs are functions of the squared sfermion masses [52]. One obtains for example [100]

$$(M_{\tilde{\nu}}^2)_{ii} \approx M_0^2 + 0.52 M_{1/2}^2 + \frac{1}{2} M_Z^2 \cos 2\beta. \quad (\text{A1})$$

On the other hand, there is also a direct proportionality of m_{ν}^{tree} to $M_{1/2}^{-1}$, *cf.* Eq. (17). All these additional effects do not significantly influence the position of the tree-level neutrino mass minimum, *i.e.* $A_0 \approx 2M_{1/2}$ still holds for $\mathbf{\Lambda} \in \{\lambda'_{ijk}\}$; see Sec. IV. However, the effects add a global slope to the terms (as a function of $M_{1/2}$), which contribute to the tree level mass. This behavior can be seen in Fig. 11.

We show in Fig. 11 the same contributions as in Fig. 3, but now as a function of $M_{1/2}$ instead of A_0 . Here A_0 has been fixed to 900 GeV. On the one hand, we observe that the quantities $\tilde{D}_i v_u$ (dotted magenta line) and $(\mathbf{m}_{H_d \tilde{L}_i}^2 + \mu \kappa_i) v_d$ (dotted-dashed blue line) are nearly constant for low values of $M_{1/2}$, but they have a positive slope for large values of $M_{1/2}$. This

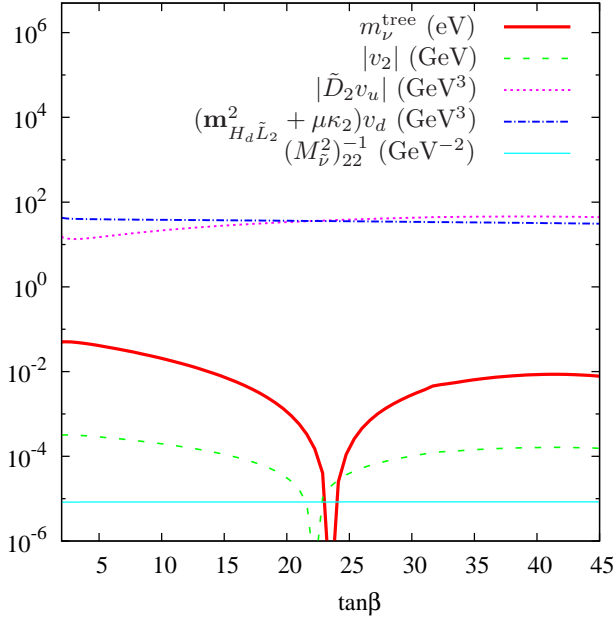


FIG. 12: Same as Fig. 3, but now for the mSUGRA parameter $\tan\beta$ instead of A_0 .

is mainly due to their dependence on μ ; *cf.* Eq. (9) [Eq. (8)] for \tilde{D}_i [κ_i]. On the other hand $(M_{\tilde{\nu}}^{-2})_{ii}$ (solid turquoise line) has a negative slope for all values of $M_{1/2}$ because of Eq. (A1). Overall this leads to a steep decrease of the tree-level neutrino mass (solid red line) in the region of low $M_{1/2}$, whereas in the region of large $M_{1/2}$, the various contributions' dependence on $M_{1/2}$ roughly cancels, see Fig. 11.

Going beyond the plot, for $M_{1/2} \rightarrow \infty$ the tree-level mass scales with $M_{1/2}^{-1}$, as follows from the different contributions to m_{ν}^{tree} in Eq. (17). Such a behavior is expected, because SUSY decouples from the SM sector in the limit $M_{1/2} \rightarrow \infty$.

2. $\tan\beta$ Dependence

Varying $\tan\beta$ most importantly affects the tree-level neutrino mass via the term $\tilde{D}_i v_u$ in Eq. (31). The RGE for \tilde{D}_i , Eq. (35), is proportional to the down-type Yukawa coupling $(Y_D)_{jk} \equiv (\mathbf{m}_d)_{jk}/v_d$. Therefore,

$$\tilde{D}_i v_u \propto c_1 + c_2 \frac{v_u}{v_d} \equiv c_1 + c_2 \tan\beta, \quad (\text{A2})$$

at M_{EW} . The factors c_1 and c_2 depend on the other mSUGRA parameters but their magnitude is approximately independent of $\tan\beta$. However, there is a dependence of $\text{sgn}(c_2)$ on $\tan\beta$ via the RGE of h'_{ijk} . Especially in case (b) of Sec. IV A, *i.e.* in the region around the tree-level neutrino mass minimum, this becomes relevant [129].

This (weak) $\tan\beta$ dependence of $|\tilde{D}_i v_u|$ is illustrated in Fig. 12 for our B₃ mSUGRA parameter set Point I; see Sec. II B. One observes that the dotted magenta line ($|\tilde{D}_i v_u|$) increases between $\tan\beta = 2$ and $\tan\beta \approx 40$. Here, $\text{sgn}(c_2) > 0$. Above $\tan\beta \approx 40$, $|\tilde{D}_i v_u|$ starts decreasing, *i.e.* $\text{sgn}(c_2) < 0$. This is due to the enhancement of the down-type Yukawa coupling when increasing $\tan\beta$, since this reduces h'_{ijk} further and further until it becomes negative. This decrease of $|\tilde{D}_i v_u|$ is only partially visible in Fig. 12 since the parameter region with high $\tan\beta$ is excluded due to tachyons.

One can also see in Fig. 12 that the other term determining the sneutrino vev, $(\mathbf{m}_{h_d \tilde{L}_i}^2 + \mu \kappa_i) v_d$, which is displayed as a dotted-dashed blue line, is fairly constant regarding $\tan\beta$. This contribution to the sneutrino vev is subtracted from the first term, $\tilde{D}_i v_u$ (dotted magenta line), so that the sneutrino vev becomes zero when the two lines intersect; see Eq. (31).

We observe this intersection in Fig. 12 at $\tan\beta \approx 22$, thus yielding the tree-level neutrino mass minimum in this region. In theory, there could even arise *two* minima because above $\tan\beta \approx 40$ $\tilde{D}_i v_u$ starts decreasing again, leading to another intersection with $(\mathbf{m}_{h_d \tilde{L}_i}^2 + \mu \kappa_i) v_d$. However, as mentioned before, this usually happens in an excluded region of parameter space.

As is also illustrated in Fig. 12, there is quite a sizable difference between the two terms which determine the sneutrino vev, *i.e.* $(\mathbf{m}_{h_d \tilde{L}_i}^2 + \mu \kappa_i) v_d$ (dotted-dashed blue line) and $\tilde{D}_i v_u$ (dotted magenta line) in the region of low $\tan\beta$. If we are looking for a neutrino mass minimum in this region of parameter space, we need to adjust A_0 towards higher values, which will increase h'_{ijk} [*cf.* Eq. (36)]. Therefore, increasing A_0 will shift the dotted magenta line upwards until it intersects with the dotted-dashed blue line at the desired low $\tan\beta$ value. This shift of the tree-level neutrino mass minimum to higher A_0 is clearly visible in Fig. 6(c). For $\tan\beta = 20$, the minimum lies at $A_0 \approx 900$ GeV whereas for $\tan\beta = 5$, it has shifted to $A_0 \approx 1300$ GeV.

3. $\text{sgn}(\mu)$ Dependence

A change of $\text{sgn}(\mu)$ notably affects the tree-level neutrino mass via the RGE running of \tilde{D}_i [Eq. (35)], in which the overall sign of the RGE is changed. Therefore, the sign of \tilde{D}_i itself is reversed at any energy scale but its magnitude is mostly unaffected. Consequently, the A_0 value where $\tilde{D}_i = 0$ is still mostly the same after a sign change.

However, at the position of the tree-level neutrino mass minimum, \tilde{D}_i needs to be slightly larger than zero in order to cancel the other terms contributing to the tree-level mass, *cf.* Sec. IV A and Sec. A 2. When we are at a parameter point where the tree-level neu-

trino mass minimum occurs for positive μ (*i.e.* \tilde{D}_i is small and positive), a sign change to $\text{sgn}(\mu) = -1$ will yield a \tilde{D}_i which is small and negative. The other contributing terms undergo no overall sign change. If we would like to obtain a neutrino mass minimum now, \tilde{D}_i needs to be increased in order to become slightly larger than zero again. This can be achieved by *decreasing* A_0 , Sec. IV A, (or, equivalently, *increasing* $M_{1/2}$, Sec. A 1) since this increases \tilde{D}_i via h'_{ijk} in its RGE, Eq. (35), when μ is negative. Therefore, the tree-level minimum will occur at smaller values of A_0 (or equivalently larger values of $M_{1/2}$) when we change $\text{sgn}(\mu) = +1$ to $\text{sgn}(\mu) = -1$.

This effect becomes more important when we go to regions of low $\tan\beta$. Here the influence of h'_{ijk} on \tilde{D}_i , Eq. (35), becomes weaker due to the decrease of the down-type Yukawa coupling, as we discussed in Sec. A 2. In order to still obtain a positive \tilde{D}_i after reversing $\text{sgn}(\mu)$, h'_{ijk} has to decrease in a more substantial fashion than for large $\tan\beta$. Therefore, the parameter point where the tree-level neutrino mass minimum is located will shift to smaller A_0 when changing $\text{sgn}(\mu) = +1$ to $\text{sgn}(\mu) = -1$, especially for $\tan\beta \lesssim 10$.

Overall, this leads to a “mirroring” of the tree-level mass minimum curve in the A_0 – $\tan\beta$ plane around $A_0 = 800 \text{ GeV} (\approx 2M_{1/2})$. This can be seen in Fig. 6(c) and Fig. 6(d): for $\text{sgn}(\mu) = +1$ the minimum shifts to higher values of A_0 with decreasing $\tan\beta$, whereas for $\text{sgn}(\mu) = -1$ the minimum shifts to lower values of A_0 .

4. M_0 Dependence

Varying M_0 does not greatly affect the tree-level neutrino mass. However, similar effects as those described in Sec. A 1 as *additional effects*, arise due to the dependence of several parameters on M_0^2 , *cf.* for example Eq. (34) and Eq. (A1). This can be seen in Fig. 13, where we again show the terms, which enter the tree-level neutrino mass formula, Eq. (17). We can see that most of the quantities depend only weakly on M_0 . This results in a nearly constant tree-level neutrino mass, *cf.* solid red line in Fig. 13.

However, the above mentioned M_0^2 dependences lead to a moderate shift of the tree-level neutrino mass minimum towards higher values of A_0 when increasing M_0 . Explaining this in detail is fairly lengthy because the M_0 dependence of the parameters determining the tree-level neutrino mass is not as straightforward as the dependence on other mSUGRA parameters. However, the effect is shown numerically in Fig. 6(b).

It should be noted that there is a similar *mirror effect* when changing $\text{sgn}(\mu)$ as for $\tan\beta$. For $\text{sgn}(\mu) = -1$, the minimum shifts towards *lower* values of A_0 when increasing M_0 .

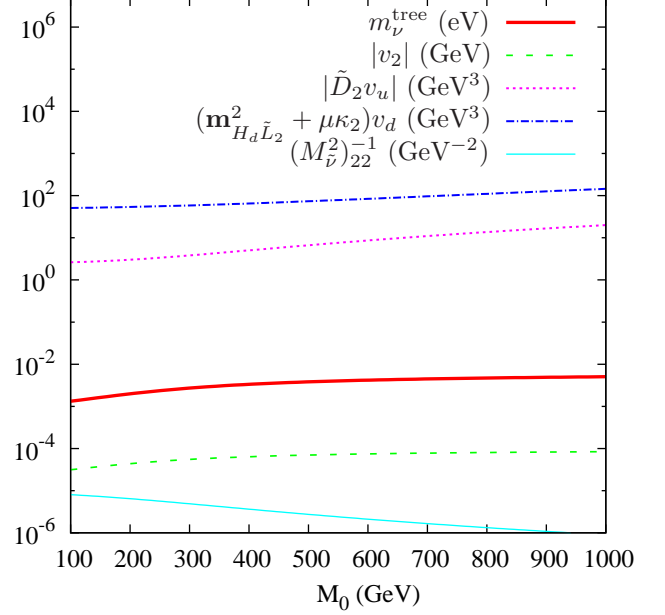


FIG. 13: Same as Fig. 3, but now for the mSUGRA parameter M_0 instead of A_0 .

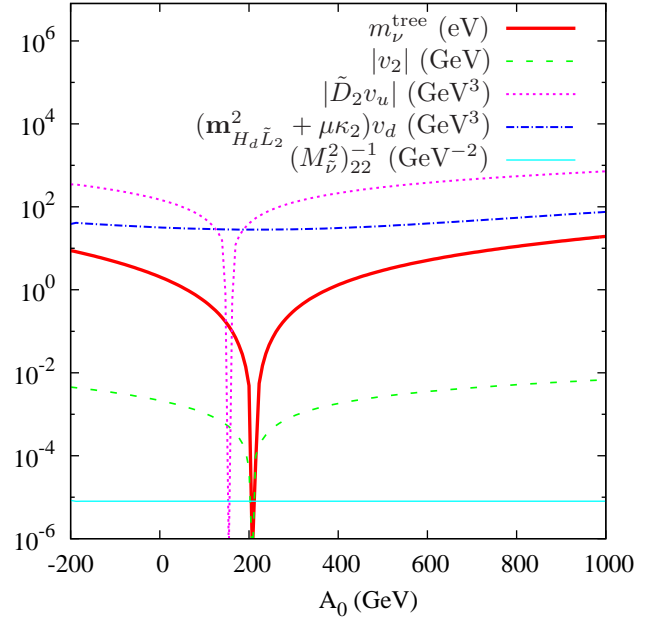


FIG. 14: Same as Fig. 3, but now for the B_3 mSUGRA Point II, Sec. II B, with $\lambda_{233}|_{\text{GUT}} = 10^{-4}$.

5. Changes for $\Lambda \in \lambda_{ijk}$

We now consider the case of $\Lambda \in \{\lambda_{ijk}\}$ instead of $\Lambda \in \{\lambda'_{ijk}\}$. Since λ_{ijk} only couples lepton superfields to each other (as opposed to the λ'_{ijk} operator which also involves quark superfields), the RGEs in Sec. IV A are reduced by a (color) factor of 3 [52, 54]. In addition, the down quark Yukawa matrix elements,

$(\mathbf{Y}_D)_{jk}$, need to be replaced by the respective lepton Yukawa matrix elements, $(\mathbf{Y}_E)_{jk}$. Otherwise, the structure of the RGEs remains the same.

The only RGE where there are more extensive relevant changes is that for h_{ijk} (which replaces h'_{ijk}); cf. Eq. (3). Eq. (36) must be replaced by [52]

$$16\pi^2 \frac{dh_{ijk}}{dt} = \frac{9}{5}g_1^2(2M_1\lambda_{ijk} - h_{ijk}) + 3g_2^2(2M_2\lambda_{ijk} - h_{ijk}) + \dots, \quad (\text{A3})$$

with $h_{ijk} = A_0 \times \lambda_{ijk}$ at M_{GUT} . This looks exactly the same as the RGE for h'_{ijk} , Eq. (36), only with g_3 and M_3 replaced by g_α and M_α ($\alpha = 1, 2$). However, it is important to realize that the running of g_α and M_α is different from the running of g_3 and M_3 . As was mentioned in Sec. IV A, the latter quantities *increase* when running to lower energy scales whereas the former *decrease* [23].

This has important consequences for the position of the tree-level neutrino mass minimum. The terms $g_\alpha^2 M_\alpha \lambda_{ijk}$ of Eq. (A3) now decrease [as opposed to $g_3^2 M_3 \lambda'_{ijk}$ in Eq. (36)]. It is thus necessary to choose A_0 smaller in order to have a smaller h_{ijk} at M_{GUT} and at lower scales to compensate for this. Quantitatively, we checked numerically that we now need $A_0 \approx M_{1/2}/2$ ($\Lambda \in \{\lambda_{ijk}\}$) to achieve a vanishing tree-level neutrino mass rather than $A_0 \approx 2M_{1/2}$ ($\Lambda \in \{\lambda'_{ijk}\}$) as was the case in Sec. IV A.

For illustrative purpose, we show in Fig. 14 the A_0 dependence of the tree-level neutrino mass (solid red line) and of the terms determining the sneutrino vev v_2 for a non-vanishing coupling λ_{233} at M_{GUT} . Fig. 14 is equivalent to Fig. 3 beside the fact that we now employ the parameter Point II with $\lambda_{233}|_{\text{GUT}} = 10^{-4}$ instead of the parameter Point I with $\lambda'_{233}|_{\text{GUT}} = 10^{-5}$, cf. Sec. II B. The qualitative behavior of all terms is the same in both figures. However, in Fig. 14 the minima are shifted to lower values of A_0 compared to Fig. 3.

We conclude that the line of argument explaining the minimum of the tree-level neutrino mass in the case of $\Lambda \in \{\lambda'_{ijk}\}$ still holds for $\Lambda \in \{\lambda_{ijk}\}$. However, the position of the minimum now shifts to

$$A_0 \approx M_{1/2}/2.$$

6. A_0 Dependence of the Neutral Scalar–Neutralino–Loops

According to Eqs. (26) and (27), the dominant loop contribution from neutral scalar–neutralino–loops to the neutrino mass matrix, $(m_{\nu}^{\tilde{\nu}\tilde{\nu}})_{ii}$, is proportional to

$$(m_{\nu}^{\tilde{\nu}\tilde{\nu}})_{ii} \propto (\tilde{D}_i v_d - \tilde{B} v_i)^2 \times f(m_{\tilde{\chi}_k^0}^2, m_{\tilde{\nu}_i}^2, m_{H_0}^2, m_{A_0}^2, m_{h_0}^2), \quad (\text{A4})$$

where f is a function of the neutralino, sneutrino and Higgs masses squared, respectively.

The A_0 dependence of Eq. (A4) is mainly determined by \tilde{D}_i , since the A_0 dependence of v_i is governed by $\tilde{D}_i(A_0)$,

$$v_i(A_0) \propto \tilde{D}_i(A_0) + c, \quad (\text{A5})$$

where the term c depends mainly on the other mSUGRA parameters but barely on A_0 , as discussed in Sec. IV A. Therefore $(m_{\nu}^{\tilde{\nu}\tilde{\nu}})_{ii}$ is roughly proportional to \tilde{D}_i^2 . The behavior of \tilde{D}_i has been discussed in detail in Sec. IV A in the context of the tree-level neutrino mass. We have shown that there is always a value of A_0 where \tilde{D}_i becomes zero. Thus the neutral scalar–neutralino loops display a similar minimum as the tree-level neutrino mass. The position of the minimum is close to the tree-level one, but not exactly aligned. This can be seen by comparing the dotted magenta line and dashed green line in Fig. 7 and Fig. 8. However, since Eq. (A4) is only an approximate formula [for the exact formula, cf. Eq. (23)], the real curve is slightly shifted downwards such that its minimum reaches negative values. Therefore $|(m_{\nu}^{\tilde{\nu}\tilde{\nu}})_{ii}|$ in Fig. 7 and Fig. 8 appears to have two minima.

It is also immediately obvious from Eq. (A4) that the scalar–neutralino–loops are roughly proportional to $[\Lambda \times (\mathbf{Y}_D)_{jk}]^2$ like the tree-level mass.

-
- [1] Y. Fukuda *et al.* [Super-Kamiokande Collaboration], Phys. Rev. Lett. **82** (1999) 2644 [arXiv:hep-ex/9812014].
 - [2] Y. Fukuda *et al.* [Super-Kamiokande Collaboration], Phys. Rev. Lett. **81** (1998) 1158 [Erratum-ibid. **81** (1998) 4279] [arXiv:hep-ex/9805021].
 - [3] Q. R. Ahmad *et al.* [SNO Collaboration], Phys. Rev. Lett. **89** (2002) 011301 [arXiv:nucl-ex/0204008].
 - [4] B. Aharmim *et al.* [SNO Collaboration], Phys. Rev. C **72** (2005) 055502 [arXiv:nucl-ex/0502021].
 - [5] M. Apollonio *et al.* [CHOOZ Collaboration], Eur. Phys. J. C **27** (2003) 331 [arXiv:hep-ex/0301017].
 - [6] B. T. Cleveland *et al.*, Astrophys. J. **496** (1998) 505.
 - [7] M. C. Gonzalez-Garcia and M. Maltoni, Phys. Rept. **460** (2008) 1 [arXiv:0704.1800 [hep-ph]]; M. C. Gonzalez-Garcia, M. Maltoni and J. Salvado, JHEP **1004** (2010) 056 [arXiv:1001.4524 [hep-ph]].
 - [8] R. Barate *et al.* [ALEPH Collaboration], Eur. Phys. J. C **2** (1998) 395.
 - [9] K. Assamagan *et al.*, Phys. Rev. D **53** (1996) 6065.
 - [10] J. Bonn *et al.*, Nucl. Phys. Proc. Suppl. **91** (2001) 273.
 - [11] V. M. Lobashev *et al.*, Nucl. Phys. Proc. Suppl. **91** (2001) 280.
 - [12] C. Amsler *et al.* [Particle Data Group], Phys. Lett. B **667** (2008) 1.

- [13] M. Cirelli and A. Strumia, JCAP **0612** (2006) 013 [arXiv:astro-ph/0607086].
- [14] A. Goobar, S. Hannestad, E. Mortsell and H. Tu, JCAP **0606** (2006) 019 [arXiv:astro-ph/0602155].
- [15] R. Wendell *et al.* [Kamiokande Collaboration], arXiv:1002.3471 [hep-ex].
- [16] P. Minkowski, Phys. Lett. B **67** (1977) 421.
- [17] R. N. Mohapatra and G. Senjanovic, Phys. Rev. Lett. **44** (1980) 912.
- [18] T. Yanagida, proc. of the Workshop: *Baryon Number of the Universe and Unified Theories*, Tsukuba, Japan, 1979.
- [19] M. Gell-Mann, P. Ramond and R. Slansky, in the proc. of the *Supergravity Stony Brook Workshop*, ed. by P. van Nieuwenhuizen and D.Z. Freedman (North Holland Publ. Co.), 1979.
- [20] R. N. Mohapatra and G. Senjanovic, Phys. Rev. D **23** (1981) 165.
- [21] M. Jezabek and Y. Sumino, Phys. Lett. B **440** (1998) 327 [arXiv:hep-ph/9807310].
- [22] H. E. Haber and G. L. Kane, Phys. Rept. **117** (1985) 75.
- [23] S. P. Martin, arXiv:hep-ph/9709356.
- [24] S. R. Coleman and J. Mandula, Phys. Rev. **159** (1967) 1251.
- [25] R. Haag, J. T. Lopuszanski and M. Sohnius, Nucl. Phys. B **88** (1975) 257.
- [26] M. Drees, arXiv:hep-ph/9611409.
- [27] E. Gildener, Phys. Rev. D **14** (1976) 1667.
- [28] M. J. G. Veltman, Acta Phys. Polon. B **12**, 437 (1981).
- [29] N. Sakai, Z. Phys. C **11** (1981) 153.
- [30] E. Witten, Nucl. Phys. B **188** (1981) 513.
- [31] L. J. Hall and M. Suzuki, Nucl. Phys. B **231** (1984) 419.
- [32] A. S. Joshipura and M. Nowakowski, Phys. Rev. D **51** (1995) 2421 [arXiv:hep-ph/9408224].
- [33] M. Nowakowski and A. Pilaftsis, Nucl. Phys. B **461** (1996) 19 [arXiv:hep-ph/9508271].
- [34] Y. Grossman and H. E. Haber, Phys. Rev. Lett. **78** (1997) 3438 [arXiv:hep-ph/9702421].
- [35] Y. Grossman and H. E. Haber, arXiv:hep-ph/9906310.
- [36] Y. Grossman and H. E. Haber, Phys. Rev. D **63** (2001) 075011 [arXiv:hep-ph/0005276].
- [37] E. Nardi, Phys. Rev. D **55** (1997) 5772 [arXiv:hep-ph/9610540].
- [38] S. Davidson and M. Losada, Phys. Rev. D **65** (2002) 075025 [arXiv:hep-ph/0010325].
- [39] A. Dedes, S. Rimmer and J. Rosiek, JHEP **0608**, 005 (2006) [arXiv:hep-ph/0603225].
- [40] H. K. Dreiner, J. Soo Kim and M. Thormeier, arXiv:0711.4315 [hep-ph].
- [41] B. C. Allanach and C. H. Kom, JHEP **0804** (2008) 081 [arXiv:0712.0852 [hep-ph]].
- [42] N. Sakai and T. Yanagida, Nucl. Phys. B **197** (1982) 533.
- [43] S. Weinberg, Phys. Rev. D **26** (1982) 287.
- [44] B. C. Allanach, A. Dedes and H. K. Dreiner, Phys. Rev. D **60** (1999) 075014 [arXiv:hep-ph/9906209].
- [45] L. E. Ibanez and G. G. Ross, Phys. Lett. B **260** (1991) 291.
- [46] L. E. Ibanez and G. G. Ross, Nucl. Phys. B **368** (1992) 3.
- [47] H. K. Dreiner, C. Luhn and M. Thormeier, Phys. Rev. D **73** (2006) 075007 [arXiv:hep-ph/0512163].
- [48] T. Banks and M. Dine, Phys. Rev. D **45** (1992) 1424 [arXiv:hep-th/9109045].
- [49] G. Bhattacharyya, Nucl. Phys. Proc. Suppl. **52A** (1997) 83 [arXiv:hep-ph/9608415].
- [50] H. K. Dreiner, arXiv:hep-ph/9707435.
- [51] R. Barbier *et al.*, Phys. Rept. **420** (2005) 1 [arXiv:hep-ph/0406039].
- [52] B. C. Allanach, A. Dedes and H. K. Dreiner, Phys. Rev. D **69** (2004) 115002 [Erratum-ibid. D **72** (2005) 079902] [arXiv:hep-ph/0309196].
- [53] S. P. Martin and M. T. Vaughn, Phys. Rev. D **50** (1994) 2282 [Erratum-ibid. D **78** (2008) 039903] [arXiv:hep-ph/9311340].
- [54] B. de Carlos and P. L. White, Phys. Rev. D **54** (1996) 3427 [arXiv:hep-ph/9602381].
- [55] T. Besmer and A. Steffen, Phys. Rev. D **63** (2001) 055007 [arXiv:hep-ph/0004067].
- [56] H. K. Dreiner and G. G. Ross, Nucl. Phys. B **365** (1991) 597.
- [57] H. K. Dreiner, P. Richardson and M. H. Seymour, Phys. Rev. D **63** (2001) 055008 [arXiv:hep-ph/0007228]; H. K. Dreiner, P. Richardson and M. H. Seymour, JHEP **0004** (2000) 008 [arXiv:hep-ph/9912407].
- [58] H. K. Dreiner, S. Grab and M. K. Trenkel, Phys. Rev. D **79** (2009) 016002 [Erratum-ibid. **79** (2009) 019902] [arXiv:0808.3079 [hep-ph]].
- [59] M. A. Bernhardt, H. K. Dreiner, S. Grab and P. Richardson, Phys. Rev. D **78** (2008) 015016 [arXiv:0802.1482 [hep-ph]].
- [60] S. Dimopoulos and L. J. Hall, Phys. Lett. B **207** (1988) 210; G. Moreau, E. Perez and G. Polesello, Nucl. Phys. B **604** (2001) 3 [arXiv:hep-ph/0003012]; D. Choudhury, S. Majhi and V. Ravindran, Nucl. Phys. B **660** (2003) 343 [arXiv:hep-ph/0207247]; L. L. Yang, C. S. Li, J. J. Liu and Q. Li, Phys. Rev. D **72** (2005) 074026 [arXiv:hep-ph/0507331]; Y. Q. Chen, T. Han and Z. G. Si, JHEP **0705** (2007) 068 [arXiv:hep-ph/0612076].
- [61] B. C. Allanach, H. K. Dreiner, P. Morawitz and M. D. Williams, Phys. Lett. B **420** (1998) 307 [arXiv:hep-ph/9708495].
- [62] M. Arai, K. Huitu, S. K. Rai and K. Rao, arXiv:1003.4708 [hep-ph].
- [63] H. K. Dreiner, S. Grab, M. Krämer and M. K. Trenkel, Phys. Rev. D **75** (2007) 035003 [arXiv:hep-ph/0611195].
- [64] B. C. Allanach, C. H. Kom and H. Pas, Phys. Rev. Lett. **103** (2009) 091801 [arXiv:0902.4697 [hep-ph]].
- [65] B. C. Allanach, M. A. Bernhardt, H. K. Dreiner, C. H. Kom and P. Richardson, Phys. Rev. D **75** (2007) 035002 [arXiv:hep-ph/0609263].
- [66] M. A. Bernhardt, S. P. Das, H. K. Dreiner and S. Grab, Phys. Rev. D **79** (2009) 035003 [arXiv:0810.3423 [hep-ph]].
- [67] H. K. Dreiner and S. Grab, Phys. Lett. B **679** (2009) 45 [arXiv:0811.0200 [hep-ph]].
- [68] I. Jack, D. R. T. Jones and A. F. Kord, Phys. Lett. B **632** (2006) 703 [arXiv:hep-ph/0505238].
- [69] H. K. Dreiner and S. Grab, AIP Conf. Proc. **1200** (2010) 358 [arXiv:0909.5407 [hep-ph]].
- [70] R. Hempfling, Nucl. Phys. B **478** (1996) 3 [arXiv:hep-ph/9511288].
- [71] D. E. Kaplan and A. E. Nelson, JHEP **0001** (2000)

- 033 [arXiv:hep-ph/9901254].
- [72] J. M. Mira, E. Nardi, D. A. Restrepo and J. W. F. Valle, Phys. Lett. B **492** (2000) 81 [arXiv:hep-ph/0007266].
- [73] M. Hirsch, W. Porod, J. C. Romao and J. W. F. Valle, Phys. Rev. D **66** (2002) 095006 [arXiv:hep-ph/0207334].
- [74] M. Hirsch, M. A. Diaz, W. Porod, J. C. Romao and J. W. F. Valle, Phys. Rev. D **62** (2000) 113008 [Erratum-ibid. D **65** (2002) 119901] [arXiv:hep-ph/0004115].
- [75] M. A. Diaz, M. Hirsch, W. Porod, J. C. Romao and J. W. F. Valle, Phys. Rev. D **68** (2003) 013009 [Erratum-ibid. D **71** (2005) 059904] [arXiv:hep-ph/0302021].
- [76] A. Bartl, M. Hirsch, T. Kernreiter, W. Porod and J. W. F. Valle, JHEP **0311** (2003) 005 [arXiv:hep-ph/0306071].
- [77] M. Hirsch and W. Porod, Phys. Rev. D **68** (2003) 115007 [arXiv:hep-ph/0307364].
- [78] M. Hirsch and J. W. F. Valle, New J. Phys. **6** (2004) 76 [arXiv:hep-ph/0405015].
- [79] M. Hirsch, W. Porod and D. Restrepo, JHEP **0503** (2005) 062 [arXiv:hep-ph/0503059].
- [80] F. de Campos, O. J. P. Eboli, M. B. Magro, W. Porod, D. Restrepo, M. Hirsch and J. W. F. Valle, JHEP **0805** (2008) 048 [arXiv:0712.2156 [hep-ph]].
- [81] F. de Campos, M. A. Diaz, O. J. P. Eboli, M. B. Magro, W. Porod and S. Skadhauge, Phys. Rev. D **77** (2008) 115025 [arXiv:0803.4405 [hep-ph]].
- [82] H. E. Haber, Nucl. Phys. Proc. Suppl. **62** (1998) 469 [arXiv:hep-ph/9709450].
- [83] L. E. Ibanez and G. G. Ross, Phys. Lett. B **110** (1982) 215.
- [84] A. H. Chamseddine, R. Arnowitt and P. Nath, Phys. Rev. Lett. **49** (1982) 970; L. Alvarez-Gaume, M. Claudson and M. Wise, Nucl. Phys. B **207** (1982) 96; L. Ibanez, Phys. Lett. B **118** (1982) 73; S. K. Soni and H. A. Weldon, Phys. Lett. B **126** (1983) 215; L. J. Hall, J. D. Lykken and S. Weinberg, Phys. Rev. D **27** (1983) 2359; R. Barbieri, S. Ferrara and C. A. Savoy, Phys. Lett. B **119** (1982) 343.
- [85] H. K. Dreiner and M. Thormeier, Phys. Rev. D **69** (2004) 053002 [arXiv:hep-ph/0305270].
- [86] B. C. Allanach, Comput. Phys. Commun. **143** (2002) 305 [arXiv:hep-ph/0104145].
- [87] B. C. Allanach and M. A. Bernhardt, Comput. Phys. Commun. **181** (2010) 232 [arXiv:0903.1805 [hep-ph]].
- [88] B. C. Allanach, M. A. Bernhardt, H. K. Dreiner, S. Grab, C. H. Kom and P. Richardson, arXiv:0710.2034 [hep-ph].
- [89] A. G. Akeroyd, M. A. Diaz, J. Ferrandis, M. A. Garcia-Jareno and J. W. F. Valle, Nucl. Phys. B **529** (1998) 3 [arXiv:hep-ph/9707395].
- [90] A. G. Akeroyd, C. Liu and J. H. Song, Phys. Rev. D **65** (2002) 015008 [arXiv:hep-ph/0107218].
- [91] J. R. Ellis, J. S. Hagelin, D. V. Nanopoulos, K. A. Olive and M. Srednicki, Nucl. Phys. B **238** (1984) 453.
- [92] S. Schael *et al.* [ALEPH Collaboration and DELPHI Collaboration and L3 Collaboration and], Eur. Phys. J. C **47** (2006) 547 [arXiv:hep-ex/0602042].
- [93] R. Barate *et al.* [LEP Working Group for Higgs boson searches and ALEPH Collaboration and], Phys. Lett. B **565** (2003) 61 [arXiv:hep-ex/0306033].
- [94] G. W. Bennett *et al.* [Muon G-2 Collaboration], Phys. Rev. D **73** (2006) 072003 [arXiv:hep-ex/0602035].
- [95] E. Barberio *et al.* [Heavy Flavor Averaging Group], arXiv:0808.1297 [hep-ex].
- [96] E. J. Chun and S. K. Kang, Phys. Rev. D **61** (2000) 075012 [arXiv:hep-ph/9909429].
- [97] S. Davidson, M. Losada and N. Rius, Nucl. Phys. B **587** (2000) 118 [arXiv:hep-ph/9911317].
- [98] A. Dedes and P. Slavich, Nucl. Phys. B **657** (2003) 333 [arXiv:hep-ph/0212132].
- [99] K. Agashe and M. Graesser, Phys. Rev. D **54** (1996) 4445 [arXiv:hep-ph/9510439].
- [100] M. Drees and S. P. Martin, arXiv:hep-ph/9504324.
- [101] H. K. Dreiner, H. E. Haber and S. P. Martin, arXiv:0812.1594 [hep-ph].
- [102] J. F. Gunion and H. E. Haber, Nucl. Phys. B **272** (1986) 1 [Erratum-ibid. B **402** (1993) 567].
- [103] A. Denner, Fortsch. Phys. **41** (1993) 307 [arXiv:0709.1075 [hep-ph]].
- [104] B. C. Allanach *et al.*, in *Proc. of the APS/DPF/DPB Summer Study on the Future of Particle Physics (Snowmass 2001)* ed. N. Graf, Eur. Phys. J. C **25** (2002) 113 [arXiv:hep-ph/0202233].
- [105] B. C. Allanach, S. Kraml and W. Porod, JHEP **0303** (2003) 016 [arXiv:hep-ph/0302102].
- [106] G. Degrandi, S. Heinemeyer, W. Hollik, P. Slavich and G. Weiglein, Eur. Phys. J. C **28** (2003) 133 [arXiv:hep-ph/0212020].
- [107] B. C. Allanach, A. Djouadi, J. L. Kneur, W. Porod and P. Slavich, JHEP **0409** (2004) 044 [arXiv:hep-ph/0406166].
- [108] J. Prades, arXiv:0909.2546 [hep-ph].
- [109] F. Jegerlehner and A. Nyffeler, Phys. Rept. **477** (2009) 1 [arXiv:0902.3360 [hep-ph]].
- [110] J. P. Miller, E. de Rafael and B. L. Roberts, Rept. Prog. Phys. **70** (2007) 795 [arXiv:hep-ph/0703049].
- [111] A. J. Buras, A. Czarnecki, M. Misiak and J. Urban, Nucl. Phys. B **631** (2002) 219 [arXiv:hep-ph/0203135].
- [112] G. Belanger, F. Boudjema, A. Pukhov and A. Semenov, Comput. Phys. Commun. **176** (2007) 367 [arXiv:hep-ph/0607059].
- [113] A. Dedes, H. K. Dreiner and U. Nierste, Phys. Rev. Lett. **87** (2001) 251804 [arXiv:hep-ph/0108037].
- [114] H. K. Dreiner, M. Kramer and B. O'Leary, Phys. Rev. D **75** (2007) 114016 [arXiv:hep-ph/0612278]; H. K. Dreiner, G. Polesello and M. Thormeier, Phys. Rev. D **65** (2002) 115006 [arXiv:hep-ph/0112228]; D. K. Ghosh, S. Raychaudhuri and K. Sridhar, Phys. Lett. B **396** (1997) 177 [arXiv:hep-ph/9608352]; G. Bhattacharyya and D. Choudhury, Mod. Phys. Lett. A **10** (1995) 1699 [arXiv:hep-ph/9503263]; Y. Kao and T. Takeuchi, arXiv:0910.4980 [Unknown].
- [115] M. Maltoni and T. Schwetz, arXiv:0812.3161 [hep-ph].
- [116] We will briefly turn to a discussion of the NLO corrections in Sect. IV C.
- [117] Mixed terms are suppressed due to our assumption of a single dominant coupling at M_{GUT} .
- [118] We use as SM inputs for SOFTSUSY the following parameters: $M_Z = 91.1876$ GeV ($m_t = 165.0$ GeV) for the pole mass of the Z boson (top quark); $\alpha^{-1}(M_Z) = 127.925$ and $\alpha_s(M_Z) =$

- 0.1176 for the gauge couplings in the \overline{MS} scheme; $m_b(m_b) = 4.20$ GeV, $m_u(2\text{GeV}) = 0.0024$ GeV, $m_d(2\text{GeV}) = 0.00475$ GeV, $m_s(2\text{GeV}) = 0.104$ GeV and $m_c(m_c) = 1.27$ GeV for the light quark masses in the \overline{MS} scheme.
- [119] Note that there is one exception, namely the direct proportionality $m_\nu^{\text{tree}} \propto 1/M_{1/2}$, *cf.* Eq. (17). However, compared to v_i , the impact of this term on m_ν^{tree} and thus on the bounds of the trilinear LNV couplings is much weaker.
 - [120] All c_i depend also weakly on $\tan\beta$. However, this becomes only relevant for very small $\tan\beta$ [100].
 - [121] Only in parameter regions with small $\tan\beta$ and small $M_{1/2}$, a term proportional to \tilde{B} , Eq. (9), becomes equally important. This is because \tilde{B} increases with decreasing $\tan\beta$ [52] whereas $\mu \times h'_{ijk}$ decreases with decreasing $M_{1/2}$, *cf.* Eq. (34) and Eq. (36). The term proportional to \tilde{B} in Eq. (9) is then enhanced with respect to the term proportional to h'_{ijk} . However, in this parameter region v_i will typically end up being negative because \tilde{D}_i is further reduced than the other term in v_i , such that the latter dominates. Then there can be no cancellation in the tree-level neutrino mass, Eq. (28).
 - [122] From Eq. (8) it is easy to see that this implies $\text{sgn}(\kappa_i) = +1$ below M_{GUT} .
 - [123] In principle, there is an A_0 dependence that stems from left-right mixing of the sfermions inside the loop, *cf.* the first term in Eq. (20). However, in most regions of parameter space we have $\mu \tan\beta \gg A_0$. In this case only the second term in Eq. (20) plays a role.
 - [124] This is clear since the LNV parameters \tilde{D}_i , κ_i and $\mathbf{m}_{h_d \tilde{L}_i}^2$ that determine the sneutrino vev are generated proportional to $\mathbf{\Lambda}$ at M_{GUT} , *cf.* Sec. IV A. From $m_\nu^{\text{tree}} \propto v_i^2$ we then obtain the relationship in Eq. (39).
 - [125] Ref. [52] did not calculate the dominant loop contributions to the neutrino mass matrix. However, these are negligible for SPS1a, because SPS1a lies far away from the tree-level mass minimum.
 - [126] This value is smaller than would be expected by estimating $A_0 \approx M_{1/2}/2 = 250$ GeV, because we are considering a parameter point with relatively low $\tan\beta$ ($\tan\beta = 10$ for SPS1a). As discussed in Sec. IV B, this leads to a shift of the tree-level neutrino mass minimum towards lower values of A_0 , *cf.* Fig. 6(c).
 - [127] Note that also the loop contributions are strongly suppressed, because the $\lambda'\lambda'$ -loops are proportional to $\lambda'_{ijk} \times \lambda'_{ikj}$, Eq. (18), and the neutral scalar loops are aligned with the tree-level mass, *cf.* Sec. A 6.
 - [128] This would change drastically if the \mathbf{Y}_E were strongly mixed [52].
 - [129] In case (a), c_2 remains always negative and in case (c), c_2 is positive.